2016

LITHOSTRATIGRAPHIC AND GEOCHEMICAL CHARACTERIZATION OF THE UPPER PENNSYLVANIAN 'WOLFCAMP D' SHALE, MIDLAND BASIN (USA): IMPLICATIONS FOR PALEOENVIRONMENTS AND UNCONVENTIONAL PETROLEUM RESERVIORS

Patrick W. Baldwin
University of Kentucky, geosciencerox@gmail.com
Digital Object Identifier: http://dx.doi.org/10.13023/ETD.2016.189

STUDENT AGREEMENT:

I represent that my thesis or dissertation and abstract are my original work. Proper attribution has been given to all outside sources. I understand that I am solely responsible for obtaining any needed copyright permissions. I have obtained needed written permission statement(s) from the owner(s) of each third-party copyrighted matter to be included in my work, allowing electronic distribution (if such use is not permitted by the fair use doctrine) which will be submitted to UKnowledge as Additional File.

I hereby grant to The University of Kentucky and its agents the irrevocable, non-exclusive, and royalty-free license to archive and make accessible my work in whole or in part in all forms of media, now or hereafter known. I agree that the document mentioned above may be made available immediately for worldwide access unless an embargo applies.

I retain all other ownership rights to the copyright of my work. I also retain the right to use in future works (such as articles or books) all or part of my work. I understand that I am free to register the copyright to my work.

REVIEW, APPROVAL AND ACCEPTANCE

The document mentioned above has been reviewed and accepted by the student's advisor, on behalf of the advisory committee, and by the Director of Graduate Studies (DGS), on behalf of the program; we verify that this is the final, approved version of the student's thesis including all changes required by the advisory committee. The undersigned agree to abide by the statements above.

Patrick W. Baldwin, Student

Dr. Michael M. McGlue, Major Professor

Dr. Edward Woolery, Director of Graduate Studies

LITHOSTRATIGRAPHIC AND GEOCHEMICAL CHARACTERIZATION OF THE UPPER PENNSYLVANIAN 'WOLFCAMP D' SHALE, MIDLAND BASIN (USA): IMPLICATIONS FOR PALEOENVIRONMENTS AND UNCONVENTIONAL PETROLEUM RESERVIORS

THESIS

A thesis submitted in partial fulfillment of the requirements for the degree of Masters of Science in the College of Arts and Sciences at the University of Kentucky

By

Patrick Webster Baldwin

Lexington, Kentucky

Director: Dr. Michael M. McGlue, Pioneer Professor of Earth and Environmental Sciences

Lexington, Kentucky

2016

ABSTRACT OF THESIS

LITHOSTRATIGRAPHIC AND GEOCHEMICAL CHARACTERIZATION OF THE UPPER PENNSYLVANIAN 'WOLFCAMP D' SHALE, MIDLAND BASIN (USA): IMPLICATIONS FOR PALEOENVIRONMENTS AND UNCONVENTIONAL

An integrated stratigraphic analysis of a ~350 ft drill core from Upton County (Texas) has revealed pervasive variability of several key siliciclastic and carbonate lithofacies in vertical section, where organic-rich siliceous mudrock beds alternate with aluminum-rich mudrocks and calcareous gravity flow deposits. Sediment chemistry, especially major and trace elements derived from x-ray fluorescence, captures this variability with high sensitivity. The high frequency chemostratigraphic variability appears to be cyclic, and it is interpreted to represent the first example of deep-water Late Pennsylvanian cyclothems for the Midland Basin. Positive trace metal (Mo, Cr) correlations to total organic carbon and gamma ray response in siliceous mudrocks, in conjunction with abundant pyrite, indicate bottom-water anoxia and possibly euxinia within the basin. The influence of glacial ice-sheets on the water level of the global ocean, in concert with local oceanographic gradients, regional tectonics, and tropical paleoclimate, constitute the primary controls on lithofacies and chemostratigraphy. The results of this study have implications for understanding the depositional history of the Midland Basin, as well as for identifying horizontal drilling zones for resource development.

KEYWORDS: Integrated Stratigraphic Analysis, Petroleum Source Rocks, Gravity Flow Deposits, Cyclothems, Unconventional Oil Reservoirs

Patrick W. Baldwin

04/22/2016

LITHOSTRATIGRAPHIC AND GEOCHEMICAL CHARACTERIZATION OF THE UPPER PENNSYLVANIAN 'WOLFCAMP D' SHALE, MIDLAND BASIN (USA): IMPLICATIONS FOR PALEOENVIRONMENTS AND UNCONVENTIONAL

By

Patrick Webster Baldwin

Dr. Michael M. McGlue

Director of Thesis

Dr. Edward Woolery

Director of Graduate Studies

April 22nd, 2016

Date

This work is in dedication to Janie Bumgarner Boland (1950-2006),
a loving mother of two taken before her time due to cancer.

“Look how far I’ve come Mom.

I’m sure you always knew I had it in me.

Love you.”

ACKNOWLEDGEMENTS

The following thesis, while an individual work, benefited from the insights and direction of several people. First, my Thesis Chair, Dr. Michael M. McGlue, exemplifies the high quality scholarship to which I aspire. In addition, Dr. Dave Moecher and Dr. Ed Woolery provided timely and instructive comments and evaluation at every stage of the thesis process, allowing me to complete this project on schedule. Each individual provided insights that guided and challenged my thinking, substantially improving the finished product.

In addition to the technical and instrumental assistance above, I received equally important assistance from family and friends. My wife, Emily Baldwin, provided on-going support throughout the thesis process critical for completing the project in a timely manner. My in-laws, Jeff and Myra Buamgardner, instilled in me, the desire and skills to obtain the Master's Degree. I wish to thank the individuals whose contributions to this project helped refine the final product and assisted with the data collection portion of this thesis, Patrick T. Ryan, Zac Perlman, and Joseph Lucas.

I would also like to thank the department of Earth and Environmental Sciences at the University of Kentucky for providing support to this project both scientifically and financially. Grants received from the department help to offset travel expenses to the Houston AAPG/SEG Student Expo where this work was awarded an honorable mention in the poster presentation portion of the meeting.

Lastly, I would like to thank Pioneer Natural Resources for donating the datasets on which this work was completed. I would also like to thank them for not only their financial assistance but their guidance and mentorship throughout the project. I would like to thank Tom Spalding and Lowell Waite for being positive role models and their contribution to this project. I would also like to thank Oliva Woodruff, Donny Loughry, Tom Deen, and Mriganko Sarkar for their contributions to the project through in house workshops in Dallas and Lexington.

TABLE OF CONTENTS

LIST OF TABLES

LIST OF FIGURES

LIST OF FILES

CHAPTER 1: INTRODUCTION

The Midland Basin, the eastern sub-basin of the Greater Permian Basin (GPB) of west Texas and southern New Mexico (Frenzel et al., 1988), has recently been the target of renewed interest for petroleum resources associated with the so-called "Great American Shale Revolution" (Waite and Read, 2014). Early exploration in the Midland Basin was solely focused on conventional low-permeability sandstone reservoirs, such as the Spraberry Formation that was discovered in 1949 (Lorenz et al., 2002; Hamlin and Baumgardner, 2012). Recent technological advancements in directional drilling and hydraulic fracturing now allow operators in the Midland Basin to produce from unconventional petroleum systems, specifically organic-rich mudrock units. Notably, Pennsylvanian and Permian source-rocks of the Wolfcamp play contain oil and gas resources that compare favorably to many unconventional plays in the onshore lower 48 states, such as the Bakken and Eagle Ford shales (Jarvie et al., 2007; Gaswirth et al., 2013). In spite of the fact that great interest surrounds the Midland Basin for its unconventional oil resources, the geology of the Paleozoic section of the basin has not been extensively reported in the literature. The cause for this is twofold. First, exposures of the deep Paleozoic section, including the Wolfcamp play, do not readily crop out in western Texas and Mexico, limiting the potential for field studies. Second, most subsurface datasets are held confidential by oil and gas companies. As a result, very little information exists in the public domain about deep Wolfcamp strata in the Midland Basin. The goal of this thesis project is to begin to address this knowledge gap through an examination of drill core stratigraphy and geochemistry of lower Wolfcamp rocks

(hereafter, “Wolfcamp D”) from the southern Midland Basin and to do so by using emerging technology for high resolution chemostratigraphic analysis.

The Permian Basin has produced oil for more than 80 years, and it is still the third largest petroleum-producing area in the United States, trailing only the Gulf of Mexico and Alaska (Dutton et al., 2005). According to the Energy Information Administration (2015), crude oil production in the Permian Basin increased from a low point of 850,000 barrels per day (bbl/d) in 2007 to 1,350,000 bbl/d in 2013. By the end of 2013, the Permian Basin accounted for ~18% of total U.S. crude oil production (Energy Information Administration, 2015). Almost three-quarters of the increase in Permian Basin crude oil production came from the Spraberry, Wolfcamp, and Bone Spring formations (Budzik and Perrin, 2014). With a resource base of this size, a better understanding of reservoir geology and advanced recovery techniques for these deep formations could have implications for energy independence in the United States (Dutton et al., 2005).

The focus of this research is a stratigraphic analysis of Wolfcamp D, a deep Paleozoic unconventional petroleum play in the Midland Basin. Wolfcamp D strata form a west and north-thinning wedge of siliciclastic sediments derived from tectonic source areas to the east and south (Hamlin and Baumgardner, 2012). Wolfcamp D siliciclastic sediments are derived from fluvial-deltaic systems prograding into the basin from the east. Another sediment source, the Marathon-Ouachita Orogen, lies to the south and east (Galley, 1958; Brown, 1969; Frenzel et al., 1988). However, lithofacies composition and thickness variability are dependent on location within the basin (Hamlin and Baumgardner, 2012). For example, basin-center areas are dominantly siliciclastic and

calcareous mudrocks, whereas shelf carbonates are more prominent along the basin margins (Adams et al., 1951; Brown, 1969; Hamlin and Baumgardner, 2012). Wolfcamp D strata differ appreciably from Upper Wolfcamp strata. In the deeper Wolfcamp D interval, siliceous mudrock facies with thin calcareous interbeds dominate in the basin-floor environments, whereas Upper Wolfcamp strata are dominantly calcareous mudrocks with local carbonate interbeds (Hamlin and Baumgardner, 2012).

The Wolfcamp D is even less well described in the literature than stratigraphically higher intervals from which oil has been produced. Yet changes in the ratio of accommodation space to sediment supply undoubtedly influenced the development of stratigraphic sequences in this mixed siliciclastic-carbonate system. Mazzullo and Reid (1989) suggested that accretionary and distally steepened ramps of the early to middle Wolfcamp interval developed during a time of alternating sea-level highstands and lowstands, concurrent with a major increase in basin subsidence. The culmination of vertical movement and deformation in the Midland Basin occurred during the deposition of the Wolfcamp Series in the Early Permian (Shumaker, 1992). Thus, the deposition of Wolfcamp D appears to have preceded maximum subsidence in the Midland Basin, and therefore accommodation may have been more localized, perhaps through karstification of the underlying Strawn Formation carbonates or differential uplift of the Central Basin Platform (Shumaker, 1992; Waite et al., 2014).

The goal of this study is to develop an enhanced understanding of the stratigraphy of Wolfcamp D, and to reconstruct paleoenvironments associated with this interval. The main hypothesis underpinning this study is that variability in stratigraphy is dominantly controlled by eustatic sea-level, driven by global paleoclimate dynamics. This study

seeks to address several key unknowns for the southern Midland Basin, including: (1) vertical stacking patterns in lithofacies; (2) mineralogical variability and the influence of diagenesis; (3) sediment chemical relationships; and (4) potential criteria for distinguishing unconventional petroleum reservoirs. The motivation for this study thus has linkages to both applied and basic geoscience research. Pioneer Natural Resources and other petroleum exploration companies view the Wolfcamp D as an unconventional shale oil play throughout the Midland Basin (Jacobs, 2013). A better understanding of paleoenvironments and a detailed stratigraphic framework will provide critical insight on reservoir characteristics of the Wolfcamp D, particularly in comparison to younger Wolfcamp intervals (Waite and Reed, 2014). To reach this goal, a combination of geochemical, lithostratigraphic, sedimentological, and petrophysical analyses have been conducted on a drill core from Upton County in the southern Midland Basin. From the academic perspective, understanding environmental controls on deposition, specifically testing hypotheses on deep-water cyclothem development, is a keen interest. Late Pennsylvanian cyclothems have been extensively studied across North America (including Kansas, Kentucky, and north Texas; Heckel, 1986; Veevers and Powell, 1987; Ettensohn et al., 1988; Boardman and Heckel, 1989; Valero Garcés, et al., 1997; West et al., 1997), but cyclothem formation in the Midland Basin is poorly known. This study allows us to begin to constrain fundamental parameters that influenced the accumulation of sediment in the basin, such as tectonics, hydrology, climate, and sea-level change.

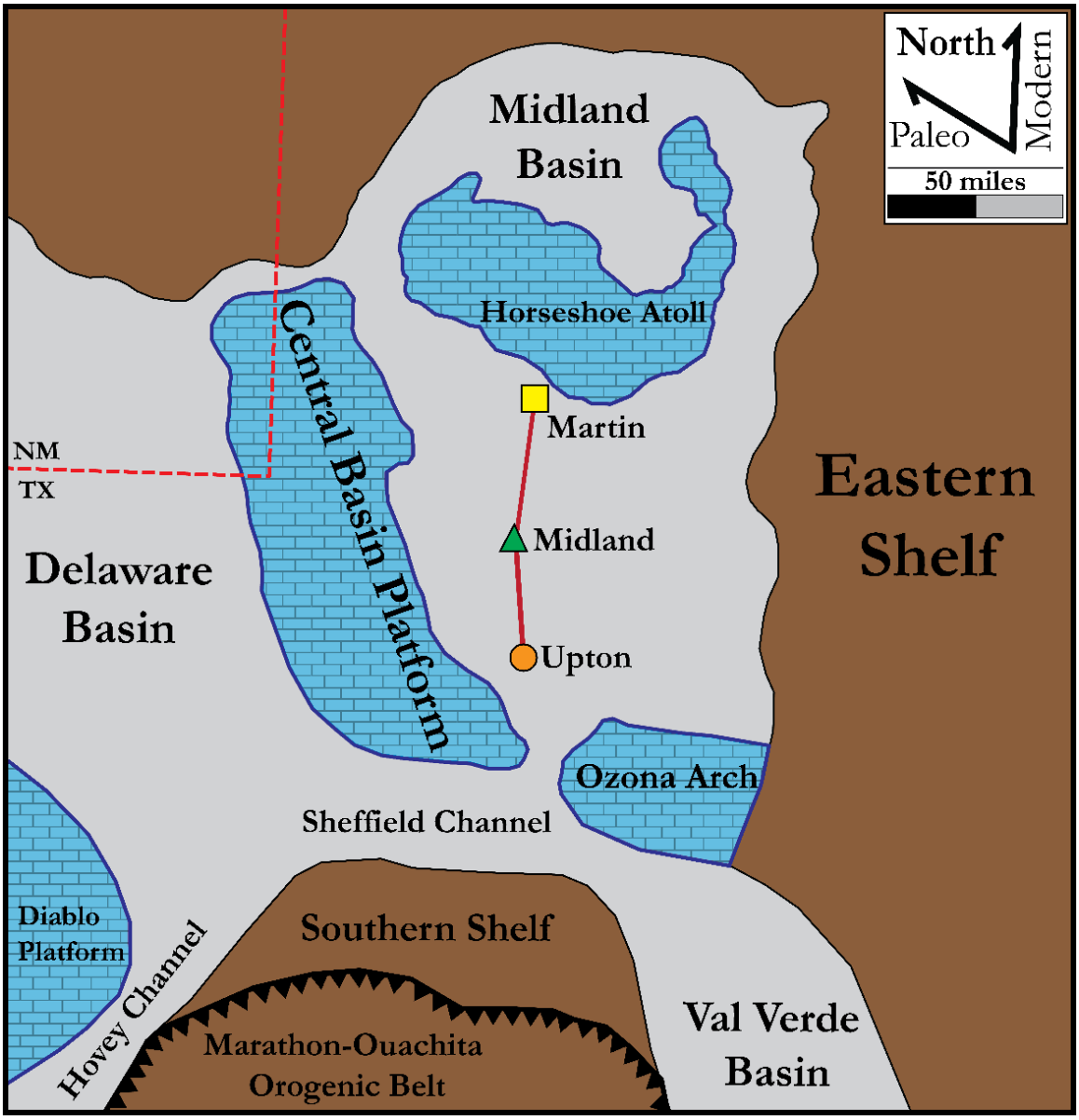

Figure 1.1. Midland Basin Base Map.
A generalized base map of the Midland Basin showing the locations of three cores obtained by Pioneer Natural Resources. These cores are on loan to the University of Kentucky Department of Earth and Environmental Sciences for the purpose of this study. This research is centered on the Upton County core, marked on the map by the orange circle. The Upton County core is located at the southern end of the Midland Basin proximal to the Central Basin Platform, Ozona Arch, and the Sheffield Channel.

CHAPTER 2: BACKGROUND

Tectonic Setting

The Permian Basin lies in the southwestern region of the midcontinental craton of North America, occupying ~115,000 mi^2 (Figure 2.1; Galley, 1958; Frenzel et al., 1988; Yang and Dorobek, 1995). The Permian Basin is comprised of two distinct depocenters that straddle a fault-bounded and uplifted central platform. This uplifted platform is known as the Central Basin Platform (CBP), and it separates the relatively deep Delaware Basin in the west from the shallower Midland Basin, positioned to the east (Figure 1.1). The Permian Basin is delimited to the south by the orogenic front of the Marathon-Ouachita Foldbelt. The eastern boundary of the Permian Basin is marked by the Bend Arch, a northward extension of the Llano Uplift (Frenzel et al., 1988). The western margin of the Permian Basin is characterized by various features, including the Guadalupe and Sacramento mountain uplifts that are positioned north and west of the Delaware Basin, respectively (Galley, 1958; Frenzel et al., 1988). The tectonic history of the Permian Basin began with the formation of the Tobosa Basin during the Early to Middle Paleozoic (Frenzel et al., 1988). The Tobosa Basin was a relatively shallow, semi-circular structural sag basin that was situated immediately east of the Diablo Uplift, south of the Matador Uplift, and west of the Texas Arch (Frenzel et al., 1988). As described by Frenzel et al. (1988), the Tobosa Basin is the heart of the Permian Basin, underlying both the Delaware and Midland Basins. Structural and topographic features defining the Tobosa Basin include the Pedernal Massif and the Concho Arch, located to the northwest and east, respectively (Galley, 1958).

The Midland Basin lies in the eastern region of the Permian Basin, adjacent to the CBP (Figure 1.1). The Midland Basin is elongate in the strike orientation (~186 mi) and narrow in the dip direction (~47 mi). The basin is oriented such that the long axis strikes approximately south-southeast to north-northwest (Figure 1.1).The western margin of the Midland Basin is marked by complex folds and faults along the eastern flank of the CBP (Galley, 1958; Yang and Dorobek, 1995; Hoak et al., 1998, Hamlin and Baumgardner, 2012). The northern limit of the Midland Basin is defined by the Matador Arch and the Palo Duro Basin, a shallow cratonic basin filled with Pennsylvanian, Permian, and Triassic sediments (Mazzullo and Reid, 1989). The eastern boundary of the Midland Basin is the eastern shelf province, comprised of carbonate platforms and prograding deltaic fan complexes (Galley, 1958; Frenzel et al., 1988; Mazzullo and Reid, 1989). The southern extent of the Midland Basin is marked by the Ozona Arch (OA), a genetically related extension of the CBP and site of an active carbonate platform during the Pennsylvanian (Shumaker, 1992). The uplifted blocks of the CBP and OA were commonly viewed as one continuous uplifted unit that later became the site of carbonate buildups that rimmed the basin margin to the west and southeast (Galley, 1958; Frenzel et al., 1988; Mazzullo and Reid, 1989; Shumaker, 1992, Hamlin and Baumgardner, 2012). In Late Mississippian time, uplift of the CBP due to the collision of Laurasia and Gondwana differentiated the Midland Basin from the Delaware Basin and the Midland Basin became a negative relief feature recognizable as a separate basin for the first time (Galley, 1958; Shumaker, 1992). According to Frenzel et al. (1988), the Midland Basin during the Pennsylvanian was marked by tectonic stability, interrupted only by occasional pulses of basinal subsidence or uplift from reactivation of the faults defining the CBP.

The uplift of the CBP ceased during Wolfcampian time, which is coincident with the earliest Permian (299 - 280 Ma; Figure 2.2).

Depositional History

Deposition within the Tobosa Basin consisted of sandstones, marls, and limestones. Sediment accumulation had begun by Late Cambrian time with the Hickory Sandstone Member of the Riley Formation. Deposition continued intermittently until the Tobosa Basin was completely filled in the Mississippian, a time span of approximately 160 Ma (Bridge, et al., 1947; Galley, 1958; Frenzel et al., 1988). Deposition of the Woodford black shale during the Late Devonian and early Mississippian marked the final stage of deposition in the Tobosa Basin (Frenzel et al., 1988).

Deposition in the Permian Basin during Mississippian time was dominantly derived from sediments eroded from the Marathon-Ouachita hinterlands to the south and east. These sediments filled adjacent foreland troughs such as the Kerr Basin, Val Verde Basin, and the Marfa Basin, and continued into the Pennsylvanian (Galley, 1958; Frenzel et al., 1988). As a result, the Midland Basin was starved of clastic sediments for most of the Carboniferous Period (Galley, 1958). The Midland Basin paleobathymetry was asymmetric and deepest in the west, along the margin of the uplifted CBP, where wells indicate ~12,000 ft of pre-Pennsylvanian strata (Galley, 1958; Frenzel et al., 1988). The basin during this time was rimmed with carbonate shelves to the east, southeast, and west and by carbonate buildups of the Matador Arch to the north (Galley, 1958; Frenzel et al., 1988). Midland Basin stratal thicknesses vary for different Mississippian-aged formations, ranging in thickness from 500 to 1,000 ft from the basin center to the basin margins. However, large areas of the Midland Basin contain strata less than 500 ft thick,

and much of the overlying Pennsylvanian rock is limestone of Desmoinesian age; Missourian and Virgilian strata are extremely thin in the Midland Basin (Galley, 1958).

Following the tectonic activity of the Mississippian Period and episodic tectonism of the Pennsylvanian, the Permian was a time of relative stability that was marked by the formation of carbonate shelves that prograded into the Midland and Delaware Basins (Galley, 1958; Frenzel et al., 1988; Hoak et al., 1998). Thick sequences of shales, siltstones, sandstones, and limestones accumulated in the depocenters of these basins by gravity flow processes and by channels that transport sediment through the marginal carbonate buildups (Frenzel et al., 1988; Mazzullo and Reid, 1989). Wolfcampian strata, which conformably overlie Pennsylvanian strata in the Midland Basin, consist mostly of grey shales with interbedded limestones and some sandstones near the basin margins (Frenzel et al., 1988).

During the Leonardian (~284 - 270.6 Ma; Figure 2.2), the deposits of the Midland Basin consisted of quartzose sandstones and siltstones that lie conformably over Wolfcampian shales (Galley, 1958; Frenzel et al., 1988). These units were deposited in deep marine waters in excess of 650 ft and comprise the Dean and Spraberry formations (Galley, 1958; Frenzel et al., 1988; Mazzullo and Reid, 1989; Hamlin and Baumgardner, 2012). The Spraberry Formation consists of fine-grained quartzose sandstones and siltstones interbedded by grey shales and occasional limestone packages (Galley, 1958; Frenzel et al., 1988). This formation is commonly known as the Spraberry Trend Oil Field and is an example of stratigraphic traps within the Midland Basin (Frenzel et al., 1988, Lorenz et al., 2002).

By Ochoan time (~260 - 251 Ma), the Delaware Basin and the Midland Basin coalesced into a single large shallow pan that was filled with thick evaporite sequences. Ochoan rocks in the Midland Basin are essentially thinner expressions of the formations within the Delaware Basin. These rocks consist of anhydrites and salts of the Salado Formation, which are overlain by red shales and sandstones of the Rustler and Dewey Lake Formations (Frenzel et al., 1988). The only exception is the absence of the Castile Formation in the Midland Basin. These Ochoan deposits act as an important regional seal that contains the diverse petroleum systems within these basins (Galley, 1958; Frenzel et al., 1988).

Paleoclimate and Oceanography

Assuming shelf biostratigraphy and correlations are accurate, the deposition of Wolfcamp D occurred during an icehouse climate of the Late Pennsylvanian (L. Waite, personal communication, 2015). This climatic state is known to have affected variations in eustatic sea-level, through the waxing and waning of continental ice sheets of Gondwanaland (Heckel, 1977; Crowell, 1978; Heckel, 1986; Boardman and Heckel, 1989; Smith and Read, 2000; Algeo and Maynard, 2003; Algeo and Heckel, 2008; Waite et al., 2014). The icehouse climate resulted from the drift of continental landmasses over Earth's poles (Crowell, 1978). The Late Pennsylvanian-Early Permian transition was a time of global climate change, and evidence indicates that the Midland Basin was located in the tropics during this interval (Figure 2.1). Paleoclimate near equatorial Pangea shifted from a more humid to semi-arid climate by the start of Permian time, and the basin appears to have been influenced by seasonal precipitation patterns (Algeo and Heckel, 2008; Tabor and Poulsen, 2008). This change in climate was the result of

orogenic processes responsible for the formation of the Central Pangean Mountains occurring on 10^6-10^7 yr time scales, overprinted by orbitally-driven glacial-interglacial cycles on the order of 10^4-10^6 yr time scales (Tabor and Poulsen, 2008). Moreover, the position of the Permian Basin proximal to the Panthalassic Ocean increased differential heating of the ocean and adjacent landmass, likely causing monsoonal climatic variability in the region (Ruddiman, 2000; Algeo and Heckel, 2008; Tabor and Poulsen, 2008). According to Parrish and Peterson (1988), most cross-bedded eolian sandstones from Permo-Pennsylvanian strata in the US southwest indicate that surface winds blew from the northeast and were the dominant pattern for latitudes between 8 - 15°N. Those authors also presented evidence for dominant wind directions originated from the north-northwest for latitudes ranging from 5 - 10°N over western Pangea. Although the exact latitudinal location for the Midland Basin is not precisely known, it is estimated to fall within 0 - 10°N paleolatitude (Figure 2.1). This suggests that both northeast and northwest winds may have blown across the Midland Basin. Additional data collected by Parrish and Petersen (1988) for eolian deposits from Lower Permian strata in Nova Scotia (0°) suggest surface wind directions from the northeast. These lines of evidence, along with modern monsoonal conditions in the northern hemisphere (Ruddiman, 2000), might suggest that northeasterly winds were the dominant wind direction experienced by the Midland Basin during the Late Pennsylvanian. However, recent model experiments suggest that the equatorial monsoon of the Late Paleozoic Icehouse may have been substantially weaker than modern analogs, with winds that were easterly or meridional (Heavens et al., 2015).

Due to its tropical latitude, the Permian Basin may have experienced seasonal precipitation that drove sediment delivery from high relief margins during the wet season (Algeo and Heckel, 2008; Figure 2.3). Strong continental runoff into the Late Pennsylvanian Midcontinent Sea (LPMS) produced a reduced-salinity surface water layer that at times may have extended into the Greater Permian Basin (Algeo and Heckel, 2008). The estuarine gyre model of oceanic circulation proposed by Algeo and Heckel (2008) in the LPMS, combined with a sub-pycnoclinal water mass close to that of normal marine salinity, created a stratified water body in the Midland Basin leading to bottom water anoxia in the deeper portions of the basin (Algeo and Heckel, 2008). Due to the proximity of the Hovey and Sheffield channels, the water column chemistry of the southern Midland Basin may have been greatly influenced by oceanic recharge from the Panthalassic Ocean (Algeo and Heckel, 2008).

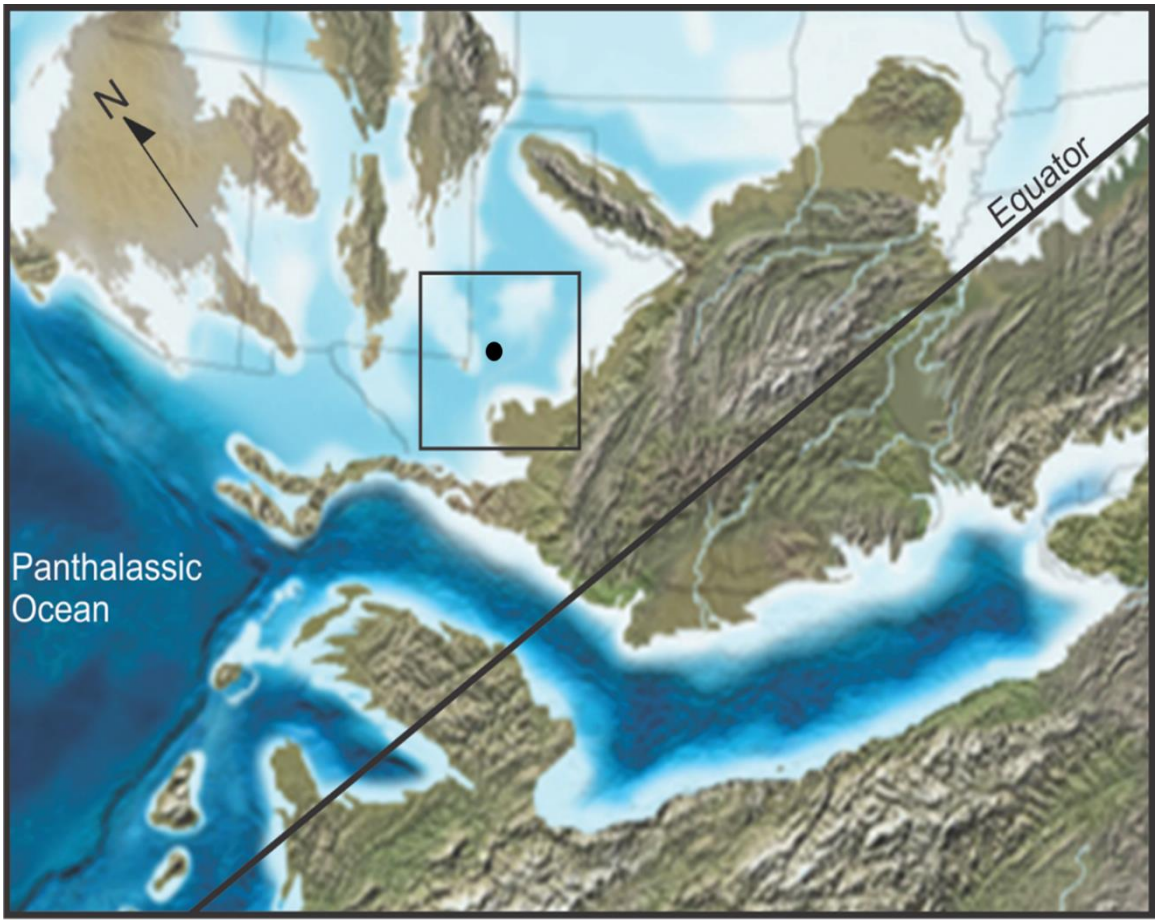

Figure 2.1. Paleogeographic Map of the Midcontinent southwest USA.
A paleogeographic map depicting the regional geological setting of the Greater Permian Basin and the surrounding southwest US approximately 300 Ma. The black square marks the location of the Permian Basin just north of the paleoequator. The black dot inside the square marks the location of the Midland Basin and the approximate location of the Upton County core. A major point of interest in this study is the connection of the Midland Basin to the Panthalassic Ocean to the west through a narrow corridor known as the Sheffield and Hovey channels. See Figure 2.3 for identification of prominent geologic features (modified from Blakey, 2013).

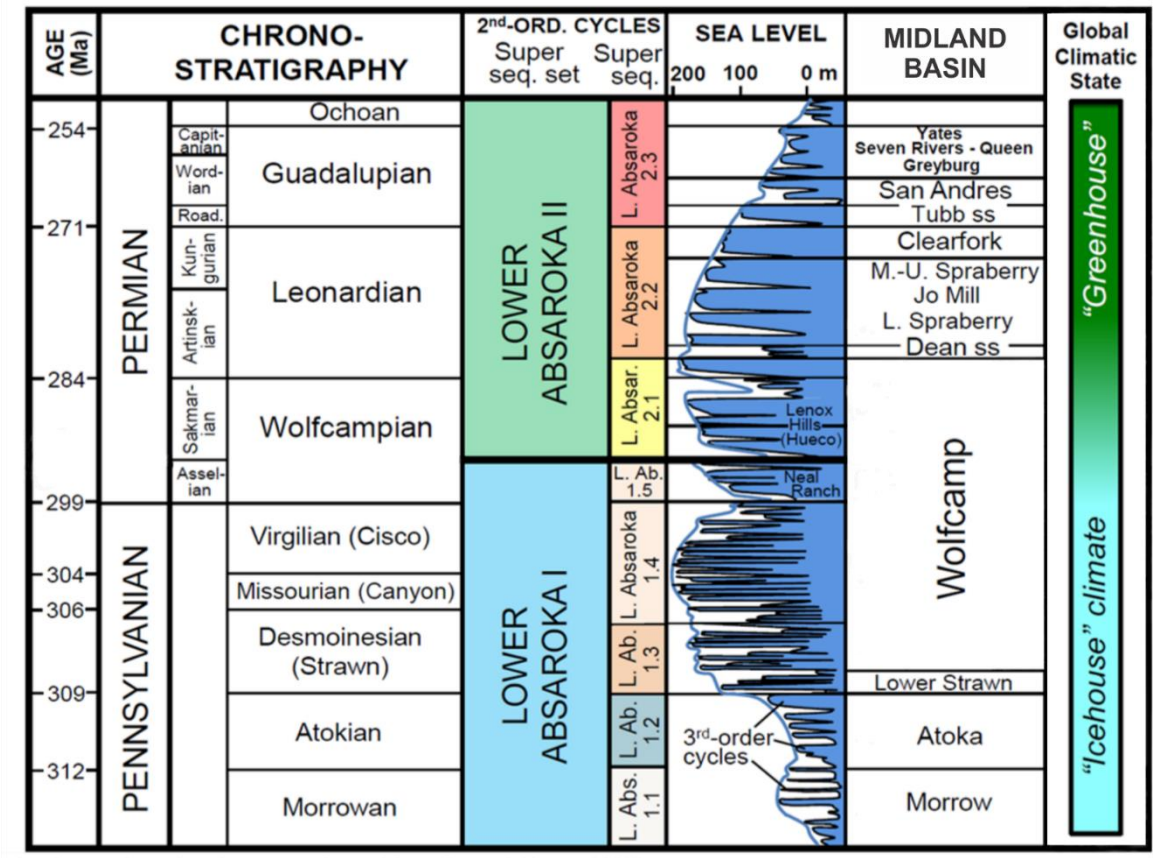

Figure 2.2. Regional Stratigraphy of the Midland Basin.
Local stratigraphy of the Midland Basin compared to the chronostratigraphy of the midcontinent southwest and super sequence cycles. Sea-level curves and Super Cycles from Sloss (1969) show the transition from Lower Absoroka 1.3 to 1.4 occurring in the lower Wolfcamp section of the Midland Basin. Additionally, the lower Wolfcampian stratigraphy of Strawn, Canyon, and Cisco time are well within the global climatic state of icehouse conditions. Modified from Waite and Reid (2014).

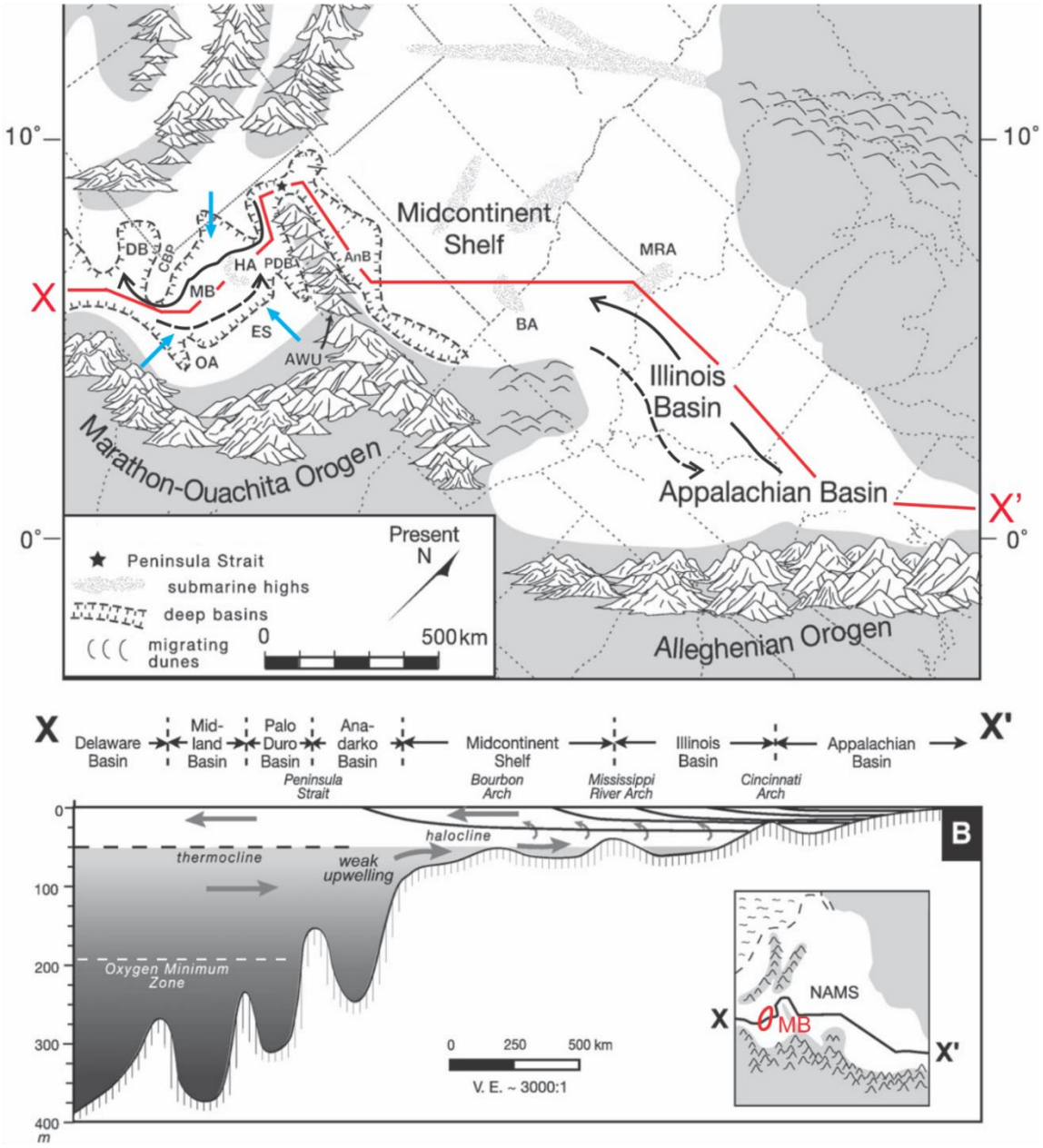

Figure 2.3. Regional Map and Cross-Section.
A) Paleogeography of the Late Pennsylvanian Midcontinent Sea (LPMS) of North America. Abbreviations: AnB=Anadarko Basin, AWU=Amarillo-Wichita Uplift, BA=Bourbon Arch, CBP=Central Basin Platform, ES=Eastern Shelf, HA=Horseshoe Atoll, MB=Midland Basin, MRA=Mississippi River Arch, OA=Ozona Arch, PDB=Palo Duro BAsin. Solid black line = surface water circulation, Dashed black line = bottom-water circulation, Blue lines = sediment sources for the Midland Basin. B) Schematic cross section X-X' from the Hovey Channel to the LPMS showing water mass circulation. Modified from Algeo and Heckel, 2008.

CHAPTER 3: METHODS

The main objective of this research is to evaluate the stratigraphy of the Upper Pennsylvanian Wolfcamp D shale using a high resolution, integrated analytical approach. A detailed assessment of facies and geochemical variability allows us to test hypotheses related to the impact of sea-level change on the Midland Basin depositional system during the Late Pennsylvanian. To this end, a number of techniques in lithostratigraphy, geochemistry, petrography, and well log analysis were applied to a drill core from Upton County (Texas). The combined result of these analyses provides insight into the composition of sediments accumulating in deep water, as well as vertical facies stacking patterns in the Wolfcamp D unit. The primary dataset available for this study was a drill core donated by Pioneer Natural Resources, which came from a well on their acreage in the southern Midland Basin (Figure 1.1). The Upton County drill core measures ~350 ft in length. The core was subdivided into five sections by Pioneer, and delivered to UK packaged in boxes, each containing five sections that measured two feet long. The core was sectioned longitudinally and polished by Pioneer contractors prior to arrival. This study was conducted on slabs that represented about 30% of the full core. The core was in good condition, and contained only minor gaps in the rocks, although a few slabs were broken into rubble.

The first step in the workflow was a lithostratigraphic analysis. Lithostratigraphy was determined by visually documenting lithology, physical sedimentary features, mineralogy, and fossil content in the core at the scale of bedding, following the approaches described by Campbell (1967), Bohacs (1990), and Bohacs et al. (2014). In certain instances, a Dino-Lite ® digital microscope was used to magnify core slabs. With

respect to lithology, initial grain size interpretations and rock types were determined through macroscopic observations and chemical reaction to dilute hydrochloric acid, which aided in the determination of carbonate content. Implementation of Dunham's classification scheme was used to describe the carbonates, which were diverse in the Upton County core (Dunham, 1962; Flügel, 2004). Rock color was determined using a Munsell soil color chart, which employs an arrangement of three dimensions of color variability including hue, value, and chroma (Munsell, 1954). However, color determinations can be biased by human insufficiencies (eyesight), moisture content of the rock, natural versus artificial light, and smoothness of the core surface (Schieber and Zimmerle, 1998). To aid in color determination, core surfaces were sprayed with water before comparison to the Munsell chart. Physical sedimentary features, such as graded bedding and scours, were identified and marked for further investigation via thin section analysis. All lithostratigraphic observations were cataloged on barrel sheets and stored in a binder for safe keeping, referencing, and iteration, following completion of the geochemical analyses.

The second step in the protocol was an analysis of inorganic sediment geochemistry. Major and trace element concentrations were determined utilizing an energy dispersive x-ray fluorescence (ED-XRF) device donated to the project by Pioneer Natural Resources (Figure 3.1a). For this purpose, the core was measured and marked at a two inch interval using orange labels (Figure 3.1b). X-ray fluorescence methodologies were adapted from Rowe et al. (2012), and utilized a Tracer IV-SD hand held device with a 40 kilo electron volts (keV) and 60 micro amperes (µA) x-ray tube. Each ED-XRF scan was made over 90 seconds, in order to improve the signal to noise ratio and assure

high quality data. The high density sample interval allowed us to track fine scale variability in lithology and geochemical signature, which is especially valuable for examining paleoceanographic proxy relationships in muddy basins influenced by high frequency environmental change (Algeo and Maynard, 2003; Rowe, et al., 2012). This scale also allows for the interpretation of microfacies that would otherwise go undetected. Major elemental analyses, which focus on elements with atomic numbers 11 through 30, were collected at 15 keV and 35 μA with a vacuum in place. Trace elemental analyses, which concerns elements with atomic numbers 20 through 51, were collected at 40 keV and 15 μA and no vacuum. To maintain internal consistency of the instrumentation and the data quality, XRF scans of unknown Wolfcamp D samples were regularly co-mingled with scans of a globally accepted shale standard, SARM41. This reference material from South Africa has been valuable for quality control, as it allows for easy identification of both systematic and random error and possible instrument malfunctions (Ring, 1989). While ED-XRF has been a useful geochemical technique for several decades, modern advances such as miniaturization and stability of the x-ray tube, optimization of spot-size and collimator, engineering of stable digital pulse processing circuitry, and software development have created the ability for lower detection limits, instrument portability, and novel approaches to fundamental parameters (Rowe, et al., 2012). With these advancements in XRF technology, the sheer quantity of data collected in a short period of time vastly improves upon older techniques (e.g., wavelength-dispersive XRF or ICP-MS). Therefore, use of the ED-XRF allows for rapid insights into elemental abundances, and the development of proxy relationships for mineralogy and total organic carbon (TOC). These relationships are used to help interpret depositional dynamics and redox

conditions in the basin. Following the ED-XRF analysis, additional sub-samples were obtained from Pioneer Natural Resources in order to complete bulk organic geochemistry, which primarily focused on total organic carbon (TOC) analyses. Understanding where intervals of enriched TOC are located in the core is critical for identifying potential hydrocarbon source rock intervals. In addition, TOC datasets provide evidence for patterns of productivity, preservation, and dilution within the basin. These parameters provide information on environmental conditions present during deposition within the basin (Sageman et al., 2008). Samples for TOC analysis were collected every five ft. The analyses were conducted at the Kentucky Geological Survey using a LECO device and a UIC Inc. total carbon coulometer. Total organic carbon was determined by subtracting total inorganic carbon (e.g., carbonate) from total carbon. Together, these methodologies provide insights on paleo-environmental conditions such as ocean chemistry, redox state, upwelling, and terrigenous inputs (Heckel, 1977; Algeo and Maynard, 2003; Rowe et al., 2012).

Petrographic analysis was conducted throughout the core via thin section analysis, with special emphasis placed on techniques for carbonates and shales. This information was used to test hypotheses on sea-level fluctuation, evaluate sedimentary processes such as gravity flows, and assess evidence for bottom water energy, position of redox fronts, and bioturbation (Schieber, 1998, 2007; Flügel, 2004; Alpin and Macquaker, 2011). Pioneer Natural Resources provided 79 mudrock and carbonate thin sections from the Upton County core, which represent a statistical sampling of the Upton County drill core. Thin section analysis was conducted on a Nikon Eclipse LV100N POL research grade petrographic microscope, using standard techniques in transmitted light microscopy.

Observations of microfabrics, mineralogy, diagenesis, and fossil content were documented and photographed (Schieber and Zimmerle, 1998). Where thin section billets or core plugs were available, an XRF scan was also collected from this material, in order to have complimentary chemistry data associated with each thin section. When possible, the XRF data was collected from the exact location of the thin section but never exceeded one tenth of an inch from that interval. Data from these locations were then used to further differentiate facies types throughout the core (Schieber and Zimmerle, 1998). This data was used as supplemental support for refining the lithostratigraphy of the Upton County drill core to ensure better accuracy and validate macroscopic observations.

Petrophysical data provided by Pioneer Natural Resources was primarily used as a supplemental proxy for lithology, and for delimiting the boundaries of the Wolfcamp D with respect to the underlying Strawn and overlying Wolfcamp C. Gamma ray logs detect formation radioactivity and allow for interpretations of rock type in the bore hole; this tool is particularly sensitive to organic rich shales. Such insights are a useful compliment to lithostratigraphy and XRF-derived geochemistry for determining paleoceanographic conditions such as bottom water oxygen and sulfide concentrations (Algeo and Maynard, 2003).

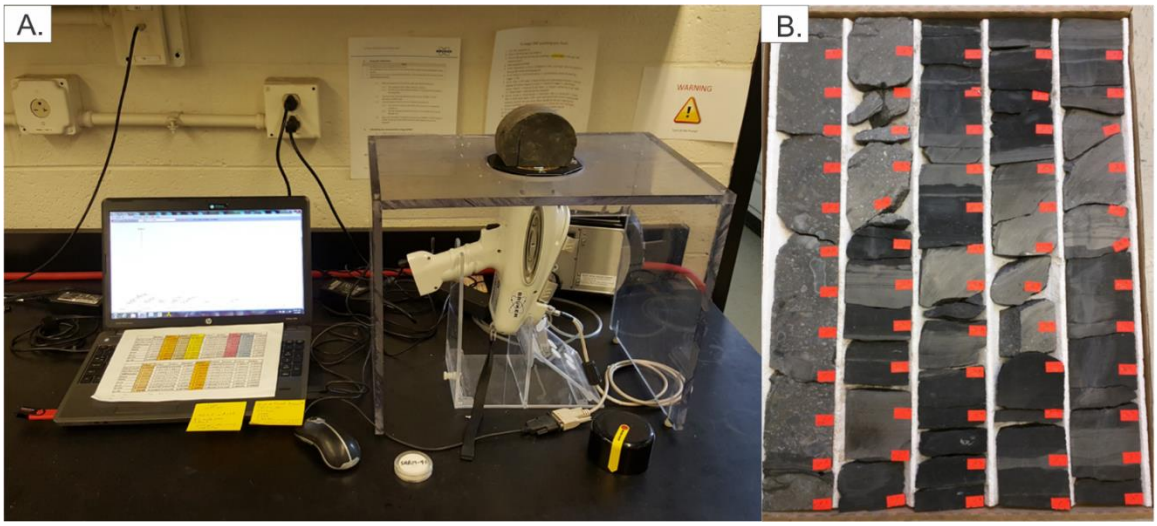

Figure 3.1. Handheld XRF setup and Labeled Core Box.
A) A Bruker handheld Tracer IV-SD X-ray fluorescence gun as used throughout this study. The Plexiglas box around the gun permitted the scanning of heavy sections of core that could not have otherwise rested atop the gun. B) A photograph of an Upton County core box marked for XRF analysis at a two inch sample interval. Note the capture of thinly bedded lithofacies in this core box marked with orange labels.

CHAPTER 4: RESULTS

Lithofacies

The Upton County drill core contains three distinct depositional units: the Strawn Formation, the Wolfcamp D (WC-D), and the overlying Wolfcamp C2 (WC-C2). Nine distinct lithofacies types were identified within these three intervals, although the focus of this project was on the mudrock-rich intervals of WC-D and WC-C2 (Supplemental Table 1). Facies types within the core vary among three types of mudrock and several types of carbonate; the distribution and thicknesses of these facies in vertical section vary dramatically (Table 4.1).

The dominant lithofacies encountered in the Upton County core were black mudrocks (Figure 4.1, Figure 4.2, and Table 4.1). Black mudrocks exist in two distinct variants (herein named black mudrock 1 [BMR1] and black mudrock 2 [BMR2]), which can be distinguished by their chemical characteristics (Supplemental Table 1). Chemically, BMR1 is characterized by low weight percentages ($\leq$6%) of aluminum (%Al) and high percentages ($\geq$26%) of silicon (%Si). These rocks are typically massively bedded. However, where bedding features were present, they consisted of continuous to discontinuous, parallel to subparallel laminations of grey silt or clay. Phosphate nodules have also been noted in BMR1; these nodules are relatively large (0.5 - 1.0 in diameter), opaque masses that lack internal structure. As a consequence of their size, these features are usually scanned by routine XRF analysis and present high percent phosphorus (%P) (Supplemental Figure 1). Displaced laminations both above and below suggests that phosphate nodules in the BMR1 lithofacies grew *in situ* around a nucleating substrate (Figure 4.3b). In thin section, perhaps the most striking feature of BMR1 is the

abundance of sand-sized *Tasmanites* cysts that are filled with quartz or pyrite (Figure 4.3c; Schieber, 1989). Pyrite, the dominant identifiable mineral in BMR1 thin sections, occurs as small nodules, fill within *Tasmanites* cysts, or as framboids dispersed within the matrix (Figure 4.3a, c). The BMR1 facies type accounts for 18 of the 79 thin sections used in this analysis and represents ~21% of the total core (351.7 ft). The distribution of BMR1 for the Strawn, WC-D, and WC-C2 intervals are 31.2%, 27.9%, and 1.13%, respectively (Table 4.1).

A second and most abundant variant of black mudrock (BMR2) is characterized by elevated values of both %Al and %Si. Macroscopically, it is very difficult to discern BMR2 from BMR1, but the differences become more obvious in thin section and in bulk chemical composition. Like BMR1, BMR2 displayed a paucity of sedimentary structures in hand sample. The BMR2 facies was commonly massive, but laminations were present occasionally. Where present, lamination were parallel to sub-parallel, continuous to discontinuous, or tilted. Observations from thin sections indicated that flattened *Tasmanites* cysts comprised many of these lamination features. Additionally, disrupted fabrics associated with burrowing were identified during thin section analysis (Figure 4.2b). These burrows varied from horizontal to sub-horizontal in orientation. The presence of calcareous fossil debris, albeit scarce, was more abundant in BMR2 than BMR1. Pyrite was abundant in BMR2, but the abundance and size of nodules was markedly less than that of BMR1. Phosphate nodules were rare to absent in BMR2. The distribution of BMR2 for the Strawn, WC-D, and WC-C2 intervals are 9.4%, 32.2%, and 56.1%, respectively (Table 4.1).

The third mudrock lithofacies identified in the Upton County core is a lighter colored variant, herein named grey mudrock (GMR). This facies type is characterized by highly variable %Al and %Si; where %Si values were typically lower than both black mudrock facies. Macroscopically, GMR is readily identifiable due to its lighter hues (GLEY2 6/10B). A distinguishing chemical characteristic of GMR is higher percentages of %Ca (~1 – 18%), which arises due to fine lime mud within the matrix. Calcareous fossil debris in the silt fraction likely also contributed to higher %Ca in the GMR, which helps to distinguish it from BMR2. Pyrite was a relatively common mineral in GMR thin sections, but total abundances were significantly lower than BMR1 and BMR2. Bedding characteristics of GMR vary depending on location in the core. Some intervals are massively bedded with few distinguishable physical sedimentary features, whereas others were marked by wavy continuous laminations. On rare occasion, beds of GMR exhibited basal scours and silty lags. The distribution of GMR for the Strawn, WC-D, and WC-C2 intervals are 38.1%, 15.1%, and 1.1%, respectively (Table 4.1).

Carbonate lithofacies encountered in the Upton County core varied in mud content, allochem types and size, bed thickness, and vertical distribution within WC-D. For example, carbonate lithofacies were relatively thin and uncommon at the base of the core, whereas a marked transition occurs at~170 ft. Above this level, carbonate bed frequency and thickness increase significantly. Average bed thicknesses of carbonate beds above this 170 ft marker are ~4 ft, while below this point average beds are ~1-2 ft thick. (Supplemental Figure 2).

Wackestones (Ws), packstones (Ps), and grainstones (Gs) were the three types of carbonate lithofacies identified in the Upton County drill core (Supplemental Table 1).

Thus, the amount of mud matrix supporting allochems varied and this characteristic was critical for drawing distinctions among the carbonate rocks (Dunham, 1962). The carbonate lithofacies all contained cemented fossil fragments and whole body fossils. Fossils that were identified in the core included bivalves, brachiopods, crinoids, foraminifera (fusulinids), gastropods, trilobites, mollusks, ostracods, and algae (Supplemental Table 1). Evidence for alteration of allochems in thin section is common, particularly replacement of calcium carbonate with silica (Figure 4.4). Other evidence of diagenesis includes dolomitized muddy matrix, which was characterized by small, blue rhombohedra and increased percent magnesium (%Mg), as well as the presence of glauconite [$(K,Na)(Fe^{3+},Al,Mg)2(Si,Al)_4O_{10}(OH)_2$] grains found within some carbonate units. Additionally, framboidal pyrite was present in all of the carbonate lithofacies types, and it occurred either as discrete grains or (rarely) replacing fossil material. Thin beds of Gs routinely presented scoured bases and normal grading. These beds occasionally contained laminations, which varied from parallel continuous to nonparallel discontinuous geometries. Low angle cross bedding was observed in several instances. These carbonate lithofacies types are very different from the Ws identified in the Upton County drill core, which contain pebble sized clasts within thicker beds. Grainstone lithofacies in thin section contained silt and sand-sized fossiliferous debris that was tightly packed and lacked interstitial lime mud. Often, the carbonate debris in beds of Gs was heavily fragmented and unidentifiable. Carbonate facies account for 17.7% of the Upton County core. The vertical distribution of Ws for the Strawn, WC-D, and WC-C2 intervals are 7.49%, 10.4%, and 14.7%, respectively (Table 4.1). The distribution of Ps for the Strawn, WC-D, and WC-C2 intervals are 0.624%, 0.829%, and 5.13%,

respectively. The distribution of Gs for the Strawn, WC-D, and WC-C2 intervals are 13.7%, 2.03Y%, and 5.61%, respectively.

Carbonate rocks found in the Upton core with elevated %Ca (≥15%) and %Mg (≥2%) values were assigned to the dolostone (M-Ls) lithofacies class. These rocks typically occur in succession with thick packages of Ws lithofacies and constitute ~3.6% of the total core. In thin section, this facies consists of massive, coarsely crystalline dolomitic matrix with occasional dispersed fossil debris (Figure 4.3d). Macroscopically, dolostone lithofacies are typically marked by longitudinal or blocky fractures, massive fabrics, and a characteristic yellow to dull orange coloration in UV light. The distribution of dolostones for the Strawn, WC-D, and WC-C2 intervals are 0.0%, 4.8%, and 1.9%, respectively (Table 4.1).

The eighth lithofacies type identified in this study has been classified as a mixed facies type (Mx). This lithofacies typically exhibits attributes of both mudrocks and carbonates, and it is characterized by wavy to folded laminations and thin beds, calcareous silt, and dispersed allochems. Macroscopically, the Mx lithofacies is readily identifiable due to the irregular bedding geometries and apparent deformation. The distribution of Mx facies for the Strawn, WC-D, and WC-C2 intervals are 0.0%, 4.5%, and 13.3%, respectively.

Occasionally, prominent authigenic and diagenetic mineral beds were encountered within the core. A particular noteworthy example was a bed of glauconite, pyrite, and phosphate grains contained within a one foot interval, stratigraphically above a package of the dolomite lithofacies (~261 - 262 ft; Figure 4.5). In another location, phosphate nodules associated with glauconite and a two inch thick pyrite bed occurred

between beds of BMR1 (below) and BMR2 (above) (~284 ft; Figure 4.6). Phosphate nodules in both stratal horizons exhibited sub-angular to angular morphology and were $\leq$ 0.5 in in diameter. These discrete beds of diagenetic minerals form the final facies type of the Upton County drill core, diagenetic mineralized beds (DMB). Other occurrences of this lithofacies type do exist in the core. These occurrences are located at ~248 ft, ~214 ft, ~200 ft, and ~130 ft and appear to be concentrated bundles of pyrite laminations.

Lithostratigraphy

As mentioned above, the Upton County core can be subdivided into three distinct depositional units. The Strawn Formation, which is predominantly a shelf carbonate that is known to have been subaerially exposed and karstified in certain areas of the Midland Basin, is typically assigned a Desmoinesian age (~309 - 306 Ma) in the greater Permian Basin. The Strawn Formation accounts for the deepest section of the core, from a depth of ~351.7 -325 ft (~26.7 ft). Overlying the Strawn Formation is the WC-D, from ~325-104 ft (~221 ft). The last depositional unit contained within the Upton County drill core is the WC-C2, from ~104-0 ft. The lithostratigraphy for the Upton County core is a complex stack of siliciclastic and carbonate lithofacies that alternate at high frequency from the base to the top of the succession. Within the Strawn, WC-D and WC-C2, a major transition in facies stacking pattern occurs at ~170 ft. At ~170 ft, beds of black mudrocks (BMR1, BMR2) become increasingly thin and more frequently punctuated by beds of carbonate lithofacies, which appear to interrupt the background muddy sedimentation (Supplemental Figure 2).

The lowest unit in the core is ~27 ft of the upper Strawn Formation. The top of the Strawn was identified using a petrophysical report donated from Pioneer Natural

Resources. The base of this interval is marked by alternating beds of BMR1 and BMR2 (Supplemental Figure 2). These mudrocks then grade vertically into a thin package of GMR, which are overlain by a thick interval of interbedded Gs with reef rubble interclasts, Ps, and Ws. The top of the Strawn interval is marked by thin GMR beds overlain by a thick package of BMR1.

Stratigraphically above the Strawn Formation lies the WC-D. This stratal package is ~221 ft thick, (~325 - 104 ft). The vertical stacking of lithofacies through the top Strawn and into the lower WC-D interval consists of a recognizable pattern of BMR1 overlain by BMR2, which in turn are capped by thick GMR, Ws and Ps beds (Supplemental Figure 2). Beds of BMR1 and GMR are appreciably thicker in lower WC-D than elsewhere in the core, and range up ~13 ft (Supplemental Figure 2). A common feature of lower WC-D was the presence of 1-2 ft M-Ls beds situated stratigraphically above GMR facies (Supplemental Figure 2). This stacking pattern is consistent from 325 - 170 ft.

Carbonates in the bottom half of WC-D (~325 - 170 ft) are dominated by the M-Ls beds. Beds of M-Ls exhibit moderately sharp to gradational contacts and in hand sample, do not present strong visible differences in grain size from the underlying GMR. However, toward approximately 185 ft, M-Ls beds become much less common, whereas thin beds of allochthonous carbonate facies become increasingly prominent (Supplemental Figure 2). Carbonate lithofacies from ~170-104 ft dominantly consist of Ws and Gs.

By contrast, in the upper half of WC-D and the overlying WC-C2 (~170 - 0 ft), BMR1 and GMR beds are typically thin, on the order of several inches to several feet

(Supplemental Figure 2). In these intervals, BMR2 beds become prominent, and in some instances they achieve substantial thicknesses (> 3 ft). This transition from BMR1 dominated mudrocks in the lower half of WC-D to BMR2 dominated mudrocks in upper half of WC-D and WC-C2 is interpreted to be one of the most significant changes in the Upton County record (Table 4.1). This stratigraphic marker occurs at ~170 ft in the core.

The WC-C2 interval in the Upton County drill core is ~104 ft thick. The WC-C2 contains all of the facies types described in the WC-D with the exception of significantly less Ws lithofacies (Table 4.1; Supplemental Figure 2). Interestingly, the percent of Ws lithofacies within the WC-C2 is ~50% less than that of the entire WC-D (~221 ft). Additionally, the percent of Ps lithofacies in the WC-C2 are two-fold greater than the amount found within the WC-D (Table 4.1). The WC-C2 is differentiated from the underlying WC-D by the amount of carbonate lithofacies and their bedding thicknesses. The M-Ls facies type are comparatively rare in WC-C2, but beds of Ps are very common. Like upper WC-D, thick beds of BMR2 and thin beds of BMR1 are present in WC-C2 (Supplemental Figure 2). The depositional pattern used to describe the upper Strawn and lower half of WC-D intervals have changed in the WC-C2. These changes are expressed as marked differences in bed thicknesses and overall diversity of lithofacies contained within the WC-C2. For example, the stacking pattern in the WC-C2 intervals is comprised of thinly bedded BMR1 facies overlain by thick occurrences of BMR2 before thinly bedded Mx and Ws to Gs facies interrupt background deposition. When this depositional pattern is compared to that of the WC-D it can be seen that the overall ordering of lithofacies is quite similar, with the exception of the M-Ls beds

(Supplemental Figure 2). The M-Ls facies occurs only once in the WC-C2, whereas this facies is more common in the WC-D (Table 4.1; Supplemental Figure 2).

Chemostratigraphy

A total of 2,095 XRF scans were collected for major and trace elements along the length of the core, providing 4,190 data points. This high resolution sampling was able to capture thinly bedded lithofacies that are often obscured or not apparent on data collected via open hole logging tools (M. Sarkar, personnel communication, 2015). Inorganic elemental variations followed lithofacies trends closely (Supplemental Figure 1 and Supplemental Figure 2).

Our primary focus for the major elements was %Al, %Ca, %Fe, %Mg, %S, %Si, and %Ti, since these elements are important constituents of the rock forming minerals (clays, calcite, ferromagnesian silicates, pyrite, and quartz). A key observation from the major element chemostratigraphy is high frequency variability, which is well illustrated in vertical plots of %Al, %Si, and %Ca throughout the ~350 ft of core (Supplemental Figure 1 and Supplemental Figure 2). This variability appears to be cyclic, although the cycles are not stationary, as their shape and frequency varies depending on the stratigraphic level (Supplemental Figure 1). In addition, the %Ca curve, which tracks carbonate lithofacies, changes from broadly defined peaks near the base of WC-D to much more narrow, high frequency peaks towards the top of WC-D. The %Mg curve is flat with occasional spikes. These excursions are correlated with large peaks in %Ca, and represent locations of the dolostone lithofacies (Supplemental Figure 1). Titanium increases towards the top of the WC-D, and it is particularly high in WC-C2. Prominent troughs in %Ti usually correlate with major peaks of %Mg and %Ca. Further, %Fe and

%S for the WC-D interval co-vary, suggesting an association in the same mineral phase (e.g., pyrite, FeS_2). At ~240 ft in the core, %Fe and %S exhibit abrupt increases and step-wise decreases for approximately four cycles to a depth of ~140 ft. These trends also track changes in TOC and molybdenum for this depth interval (Supplemental Figure 1). Values of %S in the Strawn and WC-C2 are consistently below 4.0 wt. %, while %Fe exhibits low values in the Strawn (below 4 wt. %) and moderate values in the WC-C2 (1-5 wt. %; Figure 4.3). Both %Fe and %S display high relative concentrations in the WC-D interval of the Upton County core.

Total organic carbon content was the primary focus for the organic geochemical study of the Upton County core. A total of 174 measurements were made along the core at an interval of ~4 - 5 ft. Total organic carbon values range from 0.07 - 7.4 wt. %, with values becoming progressively higher above ~300 ft in the core. Figure 4.7 shows the variation in TOC with depth for the Upton County drill core, and Supplemental Table 1 also provides the wt. % TOC values and the mean for the different facies types. Of the nine lithofacies identified in this study, the mudrocks contain the highest values of TOC. The BMR1 facies is the most organically enriched mudrock facies type and contains on average ~3.1 wt. % TOC, whereas BMR2 contains on average ~2.1 wt. % TOC (Supplemental Table 1). The most organically lean lithofacies of the Upton County drill core are M-Ls beds with an average TOC content of ~0.43 wt. % (Supplemental Table 1).

Trace metal data derived from XRF analysis shows that co-variation between molybdenum (Mo) and chromium (Cr) when cross plotted against TOC exists within the Upton County drill core (Figures 4.8, 4.9). Correlation coefficients (r^2) for Mo and Cr versus TOC are moderate to strong, ranging from 0.58 - 0.74 for Mo and 0.64 - 0.80 for

Cr. Our database of TOC and XRF data suggests that a relationship exists between organic matter content, metal concentration, and lithofacies. The BMR1 lithofacies shows the most enrichment with elevated Mo values greater than 20 ppm and TOC values above 2 wt. % (Figure 4.8).

	BMR1	BMR2	Mx	GMR	Ws	Ps	Gs	M-Ls	DMB
Total Feet	71.33	132.00	23.83	44.67	40.33	7.33	14.00	12.50	2.83
Total %	20.45	37.84	6.83	12.80	11.56	2.10	4.01	3.58	0.81
Strawn Feet	8.33	2.50	0.00	10.17	2.00	0.17	3.67	0.00	0.00
% Strawn	31.21	9.36	0.00	38.08	7.49	0.62	13.73	0.00	0.00
LWC-D Feet	30.50	10.00	0.17	13.67	3.50	0.33	0.17	7.67	1.33
% LWC-D	44.85	14.71	0.25	20.10	5.15	0.49	0.25	11.27	1.96
MWC-D Feet	24.83	28.00	2.50	16.83	3.50	0.00	2.00	0.33	1.00
% MWC-D	31.04	35.00	3.13	21.04	4.38	0.00	2.50	0.42	1.25
UWC-D Feet	6.50	33.17	7.33	2.83	16.00	1.50	2.33	2.50	0.50
% UWC-D	8.90	45.43	10.05	3.88	21.92	2.05	3.20	3.42	0.68
WC-C2 Feet	1.17	58.33	13.83	1.17	15.33	5.33	5.83	2.00	0.00
% WC-C2	1.12	56.09	13.30	1.12	14.74	5.13	5.61	1.92	0.00

Table 4.1. Facies Distribution of Upton County Drill Core.

Facies distribution data for the Upton County Drill Core was derived from all XRF data collected for the core. Constraints on chemical signatures for facies types were derived from thin section analysis and corresponding XRF scans. Based on the chemical signatures of facies types each XRF point was scrutinized and assigned a facies. Core photographs were also used in this classification. The shift in black mudrock composition is captured well in the table. Moving up section from the base of the core, a decrease in the abundance of BMR1 occurs, whereas BMR2 abundances increase. The table also shows that M-Ls facies are dominant in the lower sections of the core. Carbonate lithologies also increase moving up section in the Upton County core.

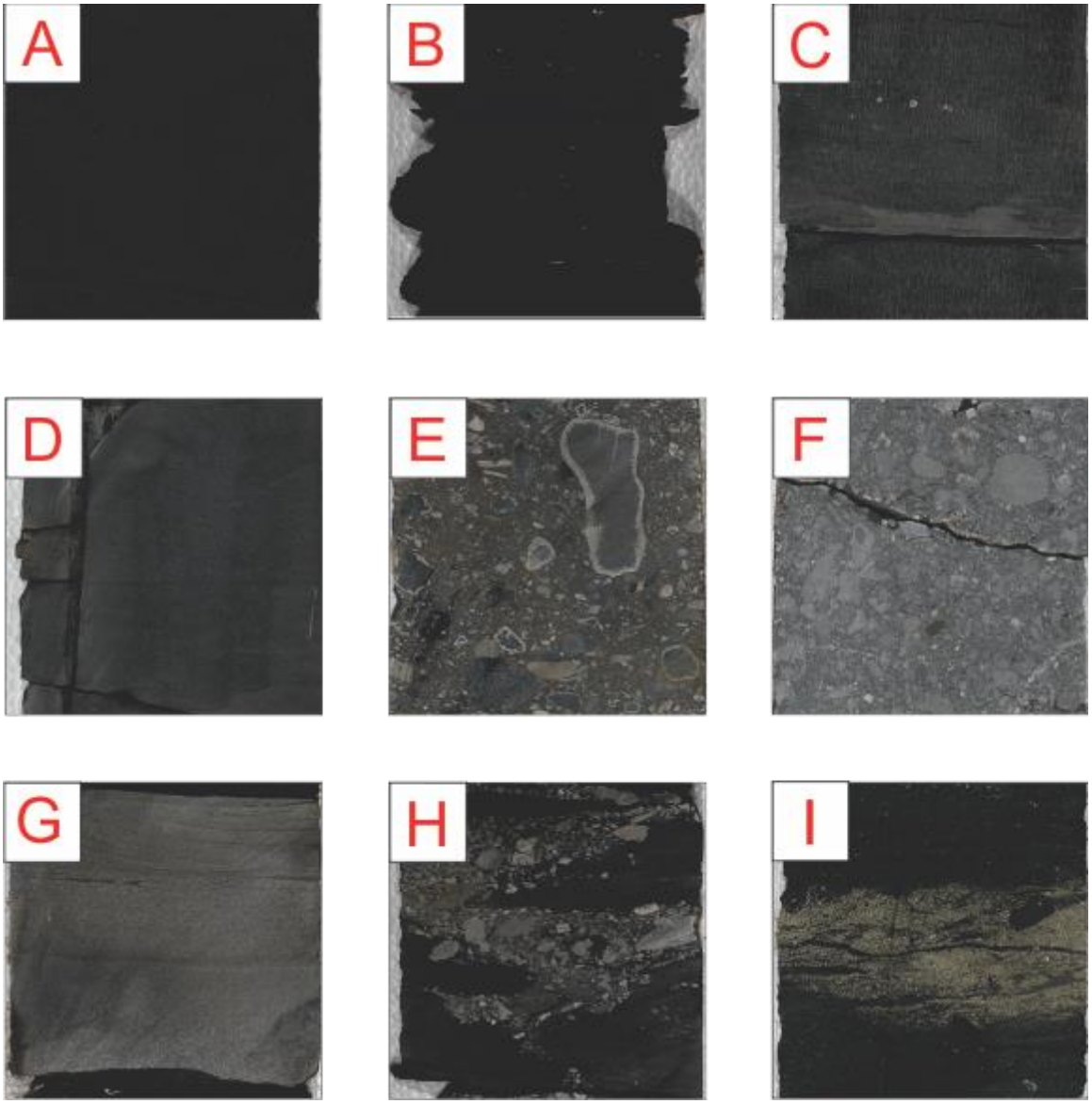

Figure 4.1. Facies Types in Hand Sample.
Photographs of the nine lithofacies types identified in the Upton County Drill Core. A) BMR1, B) BMR2, C) GMR, D) M-Ls, E) Ws, F) Ps, G) Gs, H) Mx, I) DMB. Facies codes, names, and descriptions are found in Supplemental Table 1.

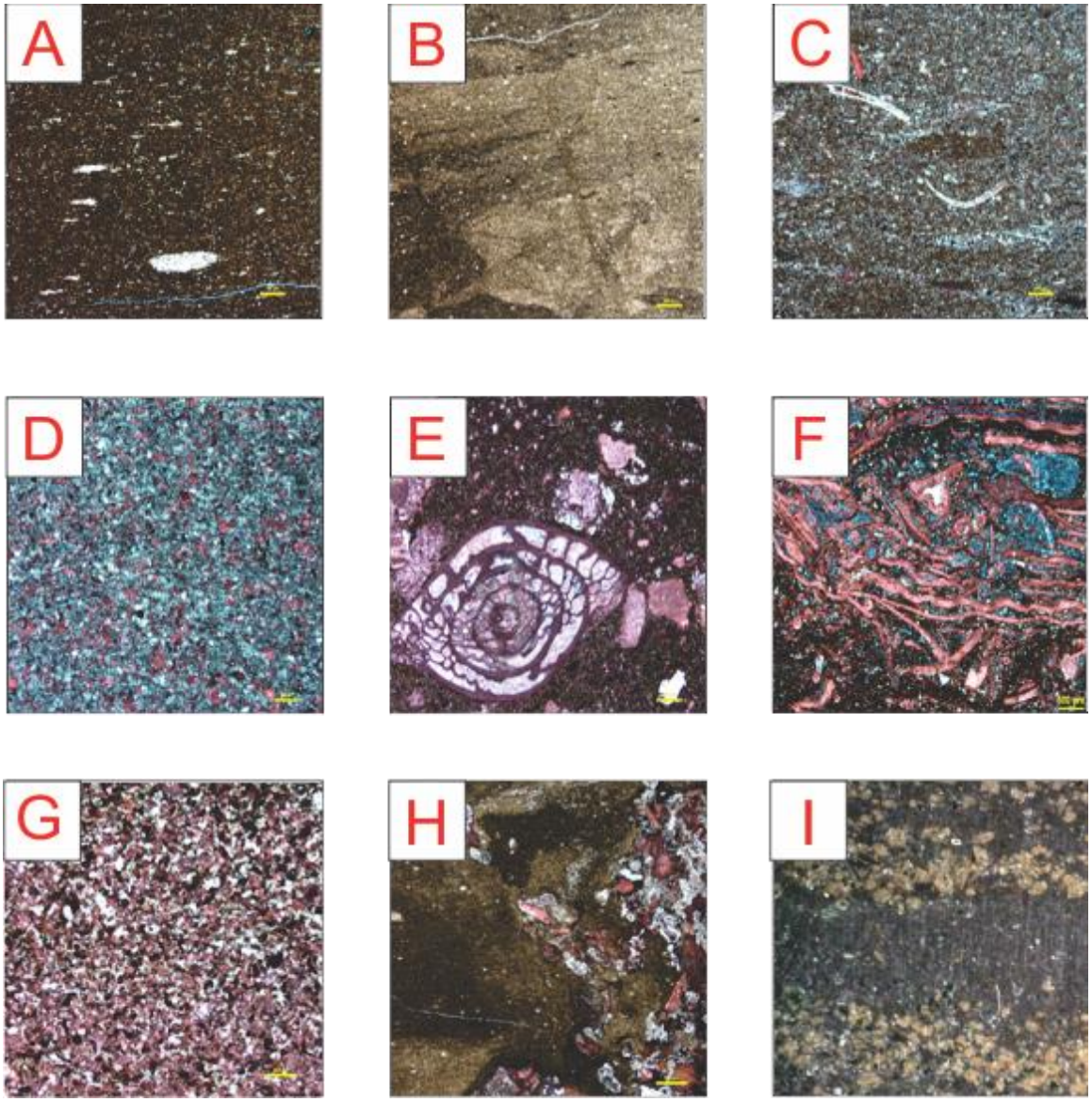

Figure 4.2. Microfacies of the Upton County Drill Core.
Photomicrographs of the nine facies types identified in the Upton County Drill Core. A) BMR1, B) BMR2, C) GMR, D) M-Ls, E) Ws, F) Ps, G) Gs, H) Mx, I) DMB. Facies codes, names, and descriptions are found in Supplemental Table 1. Since no thin sections existed for the DMB facies, images were obtained using a Dino-Lite® handheld microscope.

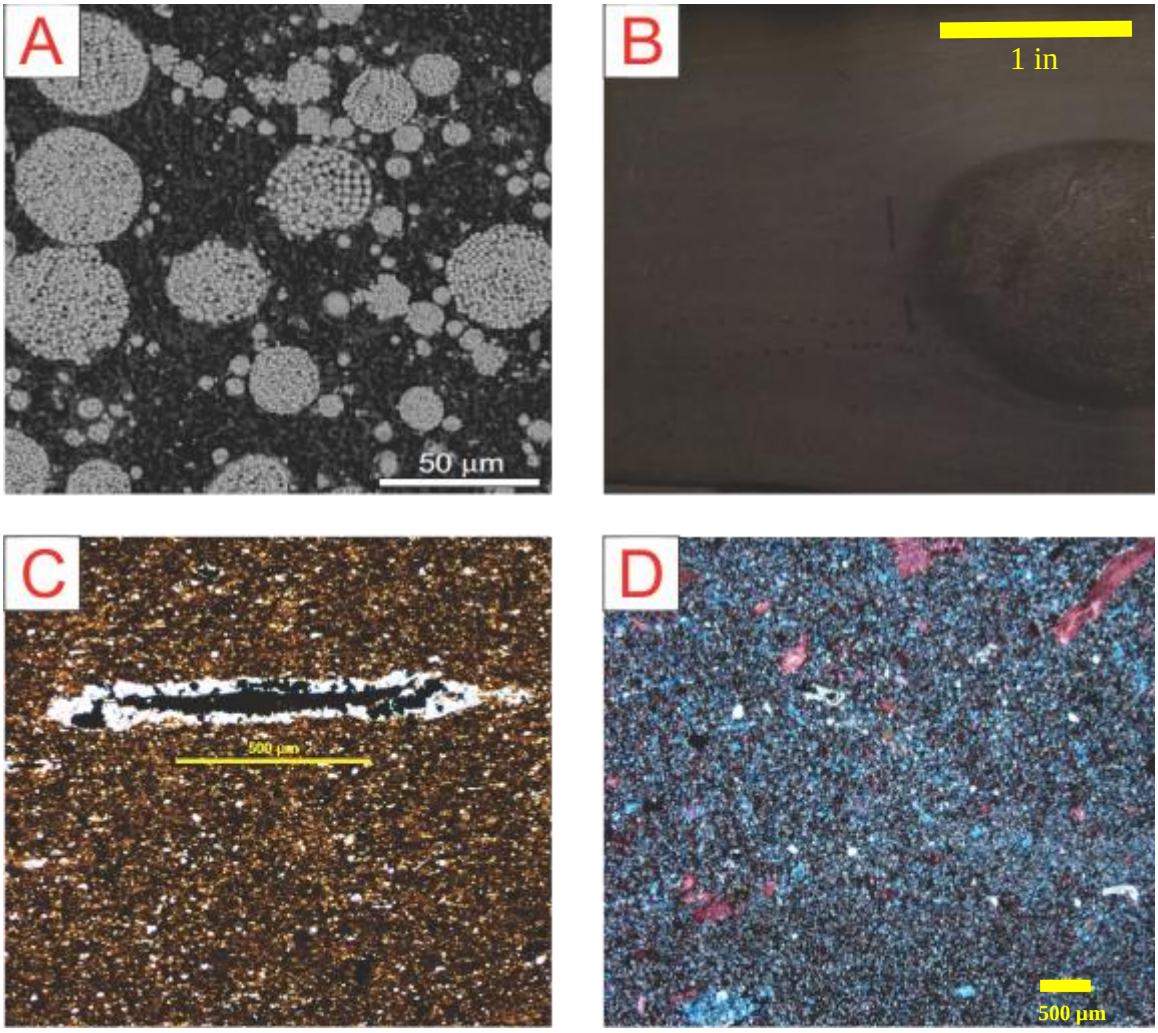

Figure 4.3. Diagenetic Mineralization.
A) Backscattered Electron image of framboidal pyrite in a siliceous mud matrix (BMR1) taken with a Cameca SX50 Probe Micro-Analyzer. B) Golf ball size phosphate nodule found in the BMR1 lithofacies. Laminations above and below the nodule are being displaced by *in situ* growth. C) Flattened *Tasmanites* cysts filled with diagenetic pyrite, scale bar = 500 microns. D) Dolostone facies (M-Ls) exhibiting diagenetic dolomitization with scattered calcareous fossil fragments.

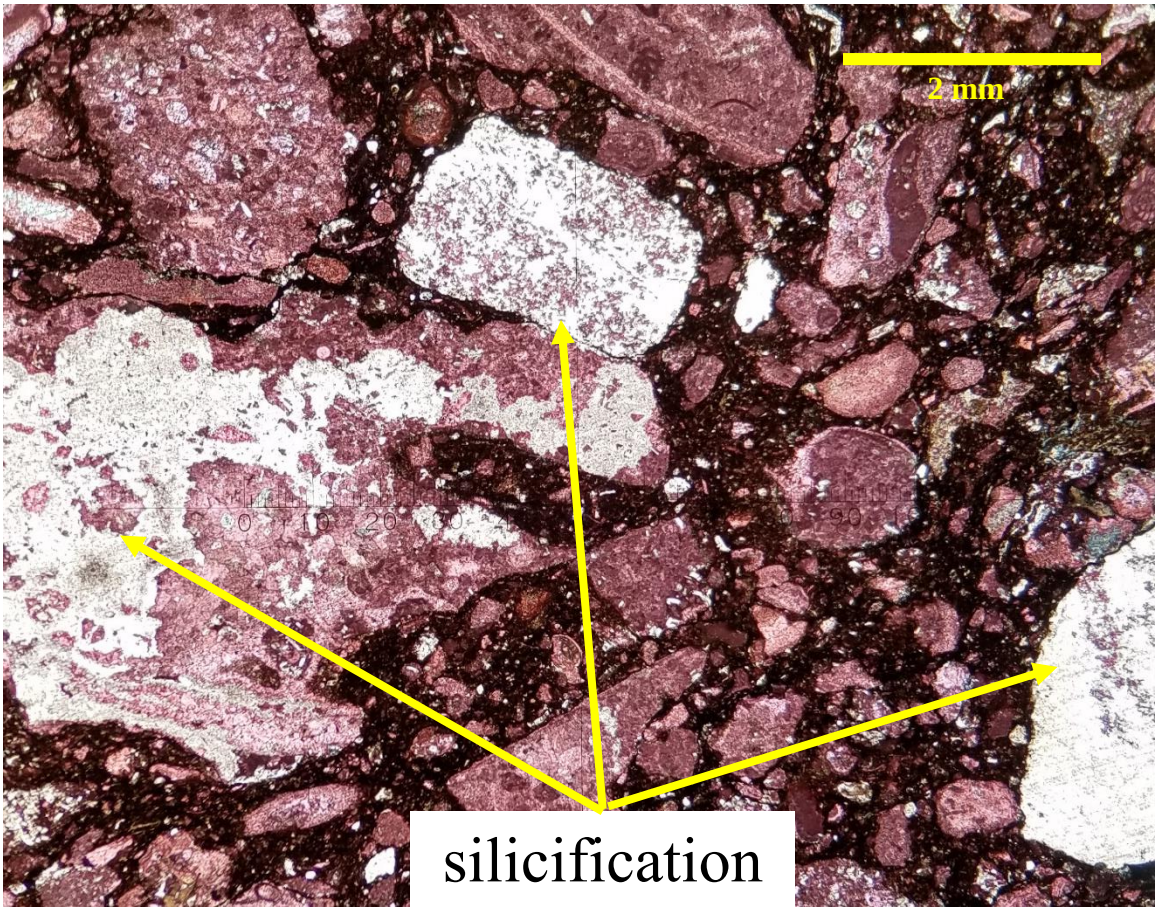

Figure 4.4. Silicification of Calcareous Fossils.
Thin section dyed with alizarin red to highlight carbonate content. Yellow arrows point to examples of silicification of carbonate sediments.

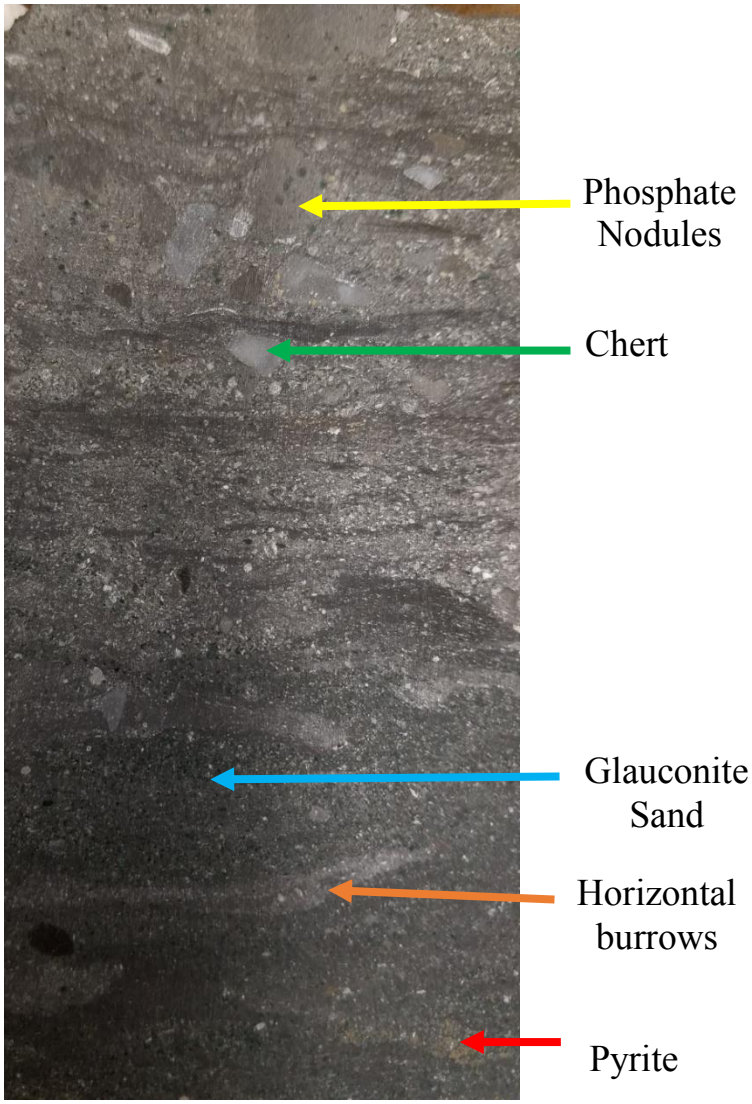

Figure 4.5. Diagenetic Mineralized Bed (DMB; ~261-262 ft).
A core photograph of the largest occurrence of the DMB facies type in the Upton County Drill Core. This 1 ft thick interval overlies a ~3 ft section of M-Ls lithofacies in the core. Sub-angular phosphate nodules (yellow arrows), angular chert clasts (green arrows), green glauconite sands (blue arrow), possible horizontal burrowing or soft sediment deformation (orange arrow), and pyrite (red arrow) are present in this interval

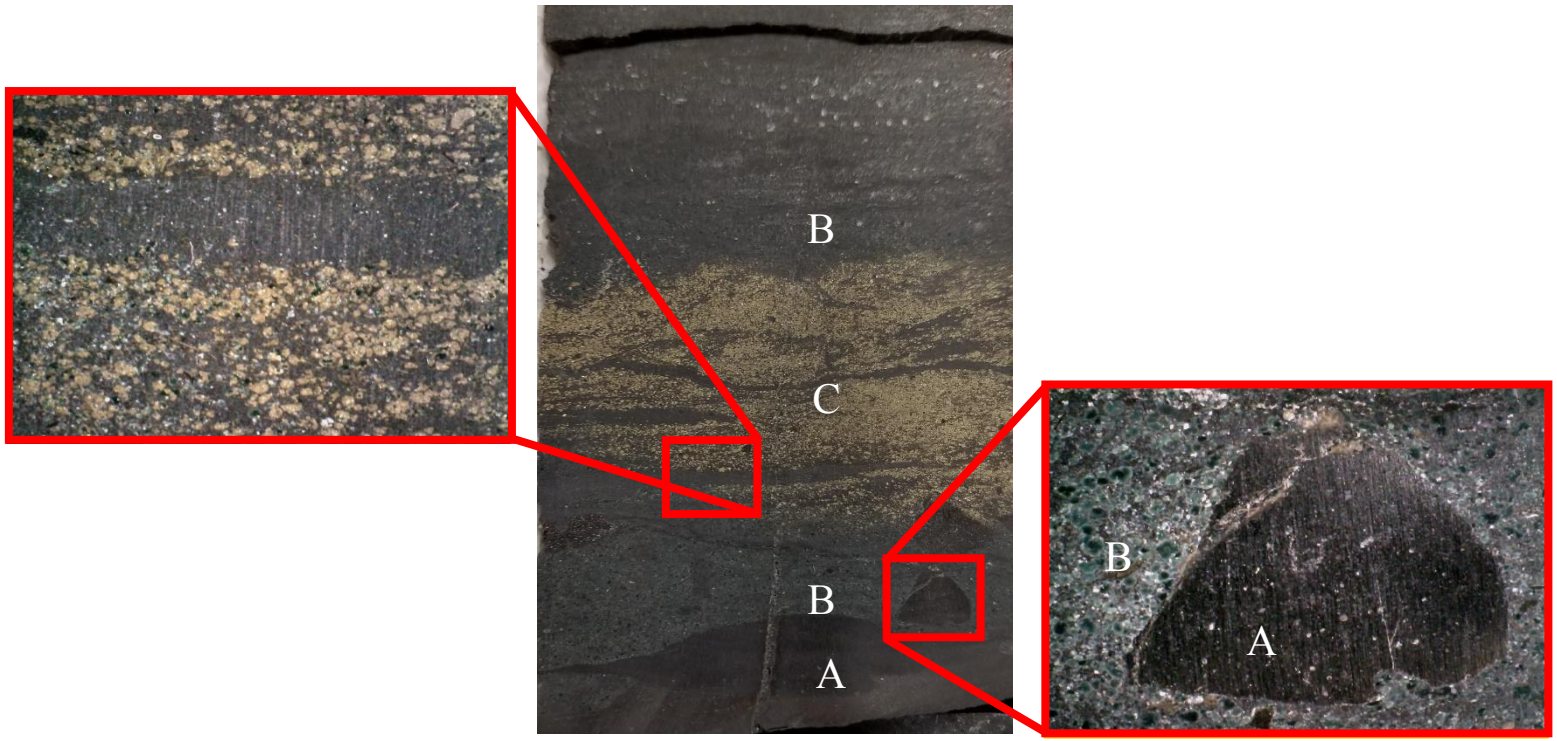

Figure 4.6. Diagenetic Mineralized Bed (DMB; ~284 ft).
Photograph of the first occurrence of the DMB facies type in the Upton County Drill core. This bed displays three prominent characteristics. A) Flattened and sub-rounded phosphate nodules, B) Glauconitic sands, and C) Abundant peloidal pyrite. At the base of this bed we observe a tapered and flattened phosphate nodule, which lies in the BMR1 lithofacies below this diagenetic bed. Stratigraphically above lies glauconitic sand with sub-rounded phosphate nodules of varying size. Just above the glauconite bed is a reworked pyrite bed consisting of peloidal pyrite grains and rare euhedral grains. Lastly, a thin bed of glauconite sand caps the bed before transitioning to the BMR2 lithofacies type.

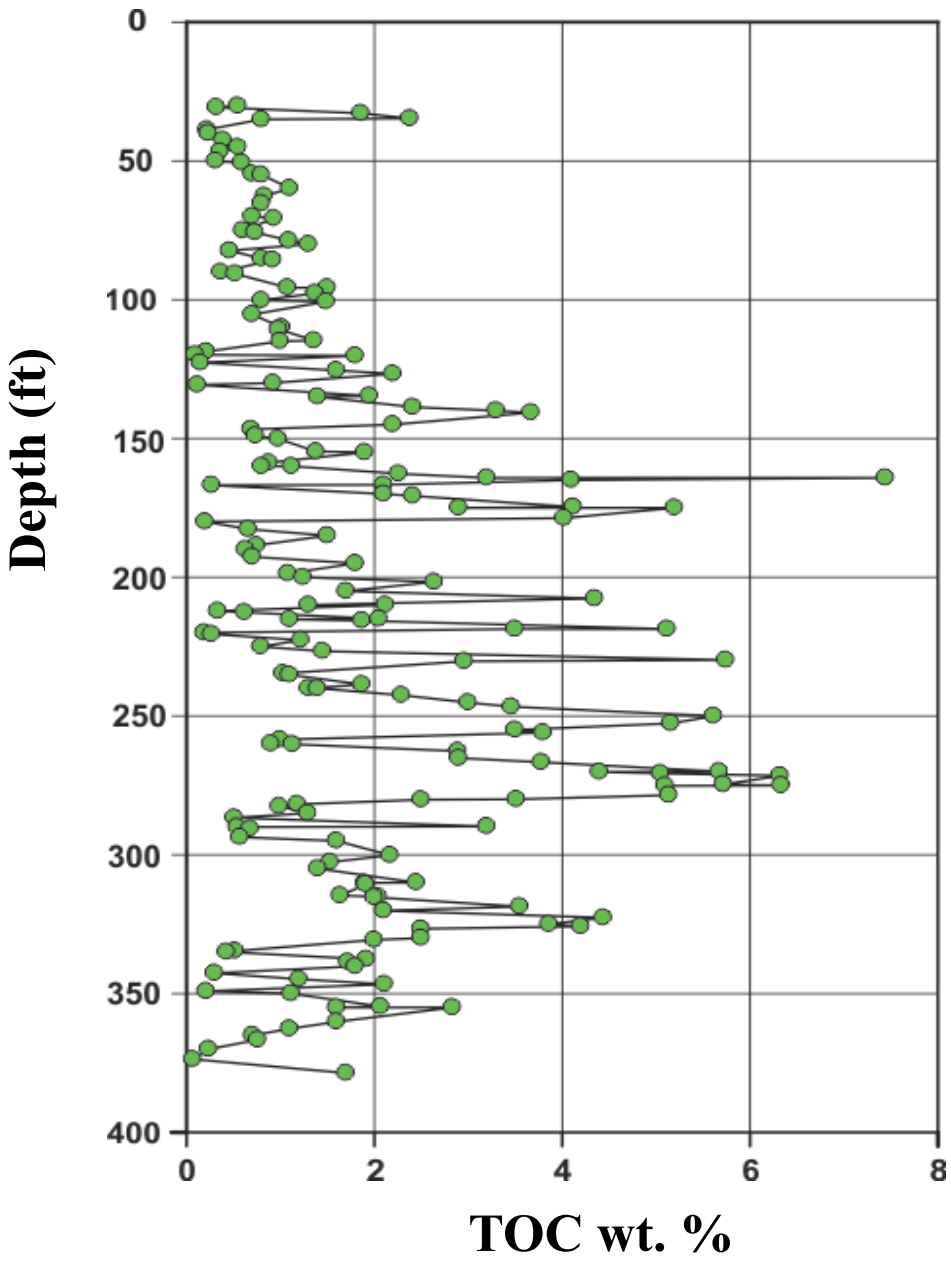

Figure 4.7. Total Organic Carbon vs. Depth.
174 measurements of TOC were collected throughout the Upton County Core. Total organic carbon values for the Upton County Drill Core fluctuate throughout the length of the core. However, the greatest values are concentrated toward the middle section of the core. Note the systematic spikey nature of the TOC values, especially in the middle section of the core. These data were used in part to identify internal sub-units in the Upton County Drill Core.

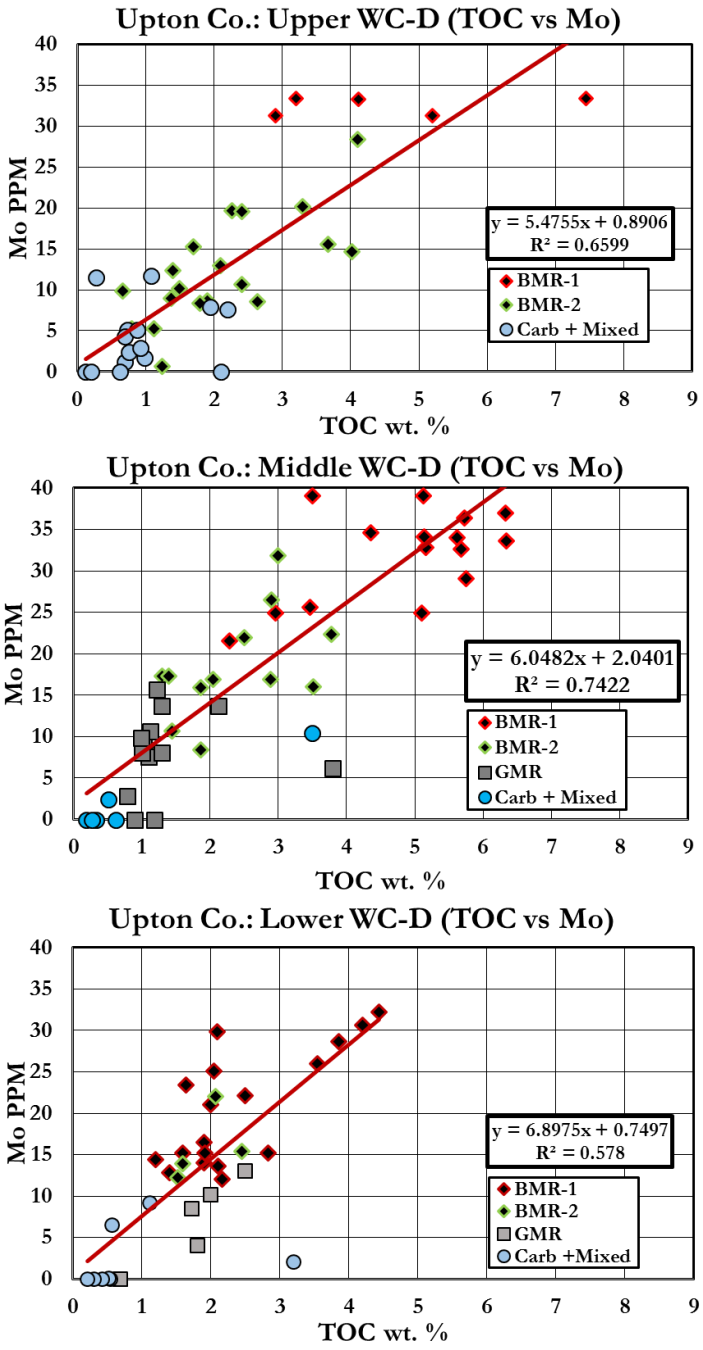

Figure 4.8. Molybdenum (Mo) vs. Total Organic Carbon (TOC) by facies.
Cross plots of Mo versus TOC show a moderate to strong correlation for the Upton County core location. These plots have been further delineated by identifying facies types and subdividing the Upton County core into a lower, middle, and upper sections. The strongest correlation is seen in the Middle Wolfcamp D (MWC-D) sub-unit then followed by the upper and finally the lower WC-D. Additionally, the BMR1 facies type tends to display the highest enrichment of Mo and TOC throughout the core.

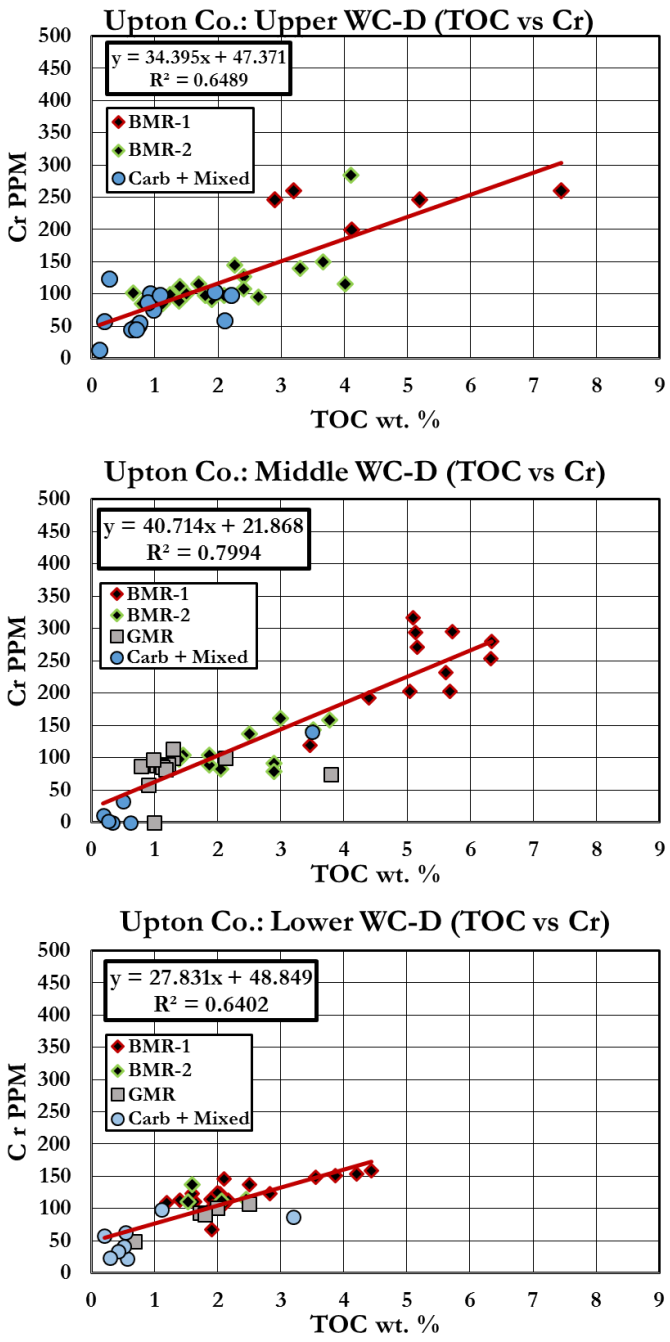

Figure 4.9. Chromium (Cr) vs. Total Organic Carbon (TOC) by facies.

Cross plots of Cr vs. TOC show a rather strong correlation for the Upton County core location. These plots have been further delineated by identifying facies types and subdividing the Upton County core into a lower, middle, and upper sections. Again, the strongest correlation is seen in the Middle Wolfcamp D (MWC-D) sub-unit then followed by the upper and finally the lower WC-D. Additionally, the BMR1 facies type tends to display the highest enrichment values of both Cr and TOC throughout the core.

CHAPTER 5: DISCUSSION

Controls on Lithofacies

The BMR1 facies type in the Upton County drill core is a black, organic rich, siliceous mudrock. This facies type lacks pervasive laminations and fissility, which are criteria that Potter et al. (2005) use for characterizing true shales. For example, there are striking differences in fabric between the WC-D BMR1 lithofacies versus the papery Devonian Ohio Shale that outcrops in central and eastern Kentucky (Ettensohn et al., 1988). The massive bedding associated with BMR1 provides compelling evidence against its characterization as a shale. Although laminations are scarce, they do occasionally occur as structures comprised of biogenic silica and pyrite. The silica present in these laminations appears to have been precipitated into *Tasmanites* cysts, most likely following the dissolution of radiolarians and sponge spicules during burial and heating. Microfacies analysis clearly shows flattened *Tasmanites*, which are aligned and oriented into discontinuous laminations in BMR1, similar to the features described by Schieber (1989, 1996). The abundance of biogenic silica suggests that surface waters were productive during the deposition of BMR1, an interpretation that is further supported by high TOC concentrations (Figure 4.8 and Figure 4.9). The abundance of early diagenetic pyrite contained within BMR1 is consistent with organic-rich sediment and Fe-rich pore waters; these conditions allowed for bacterial sulfate reduction to take place in sediment pore space (Taylor and Macquaker, 1999; Scott and Lyons, 2012). Additional lines of evidence that suggest pyrite was mineralized during early diagenesis of the BMR1 facies are the diverse morphologies of pyrite observed in thin section. The dominant pyrite morphology in BMR1 is framboidal (Figure 4.3a), with only minor

occurrences of micron-sized euhedral crystals that tend to form later in burial diagenesis (Scott and Lyons, 2012). The abundance of pyrite and TOC in BMR1 suggests that bottom waters were anoxic and possibly euxinic during deposition (Scheiber, 1996; Bohacs, 1998; Potter et al., 2005; Scott and Lyons, 2012).

Detrital silt (dominantly quartz) exists in BMR1, but these grains comprise <10% of the total matrix based on observations made from thin sections. This characteristic strongly contrasts with Devonian-Mississippian black shales deposited in the Appalachian Basin, which are comprised of siliciclastic detritus (Ettensohn et al., 1988). Another important characteristic of BMR1 is the occurrence of large (<1 in) rounded phosphate nodules (Figure 4.3b). The presence of these nodules highlights laminations in some instances, which were deformed and displaced as the nodule grew *in situ* within the muddy matrix. The BMR1 facies exhibits the highest average TOC concentrations, trace metal concentrations (Mo, Cr), and spectral gamma ray response measured in this core for all lithofacies types identified.

Taken together, the sedimentary, geochemical, and petrophysical characteristics of BMR1 are consistent with deposition during an interval when sea-floor oxygen levels were at a minimum in the Midland Basin. The high frequency recurrence of BMR1 throughout the core demonstrates that these bottom water redox conditions occurred at least quasi-cyclically during the deposition of Wolfcamp D (Supplemental Figure 2). We interpret that these environmental condition were most likely produced during sea-level lowstands. Several lines of evidence suggest that deposition of BMR1 was associated with bottom water anoxia, and possibly euxinia. In their study of the Late Pennsylvanian Midcontinent Sea (LPMS), Algeo and Heckel (2008) noted that paleoceanographic

circulation patterns likely favored anoxia in the Midland Basin. According to these authors, density stratification of the water column (via a well-defined thermocline) resulted from warm, freshwater runoff from the continental margins capping preconditioned, oxygen-depleted water from the Panthalassic Ocean. Elevated wt. % TOC content in BMR1 are interpreted to result from high primary productivity coupled with conditions at the sediment-water interface that favor preservation of organic matter (Bohacs, 1998; Sageman et al., 2003). Microfacies characteristics, namely the presence of recrystallized biogenic silica filling *Tasmanites* (Figure 4.3c), as well as wt. % TOC, provides evidence for productive surface waters during the deposition of BMR1. The elevated silica values observed in BMR1 (>26 wt. %) can be explained by gravitational settling of siliceous tests onto the sea floor, where they accumulate, become buried, and ultimately dissolve (Schieber, 1989; Schieber, 1996; Potter et al., 2005). The proliferation of Radiolarians, which are zooplankton with siliceous tests and also primary consumers of photosynthetic marine algae, are likely associated with higher algal productivity in the surface waters. This increased productivity in the upper water column may account for increased organic matter deposition in BMR1 facies types (Bohacs 1998; Sageman et al., 2003). Increased organic productivity in the photic zone of the Midland Basin could lead to increased preservation of organic carbon based on the overabundance of organic material falling to the sea floor and localized sedimentation rates for this core location (Galley, 1958; Frenzel et al., 1988; Algeo and Maynard, 2004). If bottom waters were indeed anoxic and euxinic, as our trace metal data suggest, the preservation potential of organic material must have been particularly high, because oxidation and bioturbation should be strongly curtailed in this environment. The Midland Basin has

been described by Galley (1958) and Frenzel et al. (1988) as a sediment-starved basin during the Late Pennsylvanian time. With a decrease in sedimentation rates during the deposition of BMR1, the potential for dilution of organic carbon from detrital influx is low, which favors rocks with higher wt. % TOC (Algeo and Maynard, 2004).

Primary productivity in the Midland Basin appears to have been an important factor in the development of organic-rich BMR1, and nutrient loads play an important role in governing phytoplankton biomass in the oceans (Bohacs, 1998; Sageman et al., 2003). Three possible pathways for delivery of bio-limiting nutrients (K, N, P) into the basin are: (1) fluvial transport of weathered solutes, sediments, and organic matter from adjacent landmasses; (2) upwelling of colder, nutrient rich waters due to wind shear along surface waters; or (3) bathymetrically derived upwelling, due to localized relief of the basin floor from the advection of oceanic currents into the southern Midland Basin (Bohacs, 1998; Algeo and Heckel, 2008). Nutrients transported into the basin by rivers draining the Marathon-Ouachita Orogen to the south and east of the core site is one possible pathway for nutrient supply to the basin (Fisher and Sarnthein, 1988). Due to its position in the tropics, the monsoon climate influencing the Midland Basin may have influenced the effect of river discharge into the basin, leading to episodic nutrient delivery to the surface waters during wet seasons (Ruddiman, 2000; Algeo and Heckel, 2008).

An alternative hypothesis for increased productivity in the surface waters of the Midland Basin and perhaps working in conjunction with the weathering of continental rocks is internal nutrient cycling via upwelling. Phosphate nodules in the BMR1 facies indicate that possible upwelling of cold, nutrient-rich oceanic water may have been able

to reach the photic zone periodically during the Late Pennsylvanian (Heckel, 1977; Kidder, 1985; Marshall-Neil and Ruffell, 2004). One possible mechanism for upwelling could be the erosion of the thermocline and partial overturn of the water column, possibly due to wind-driven Ekman transport of surface waters across the basin (Ruddiman, 2000; Algeo and Heckel, 2008). A second possible mechanism for upwelling is the influx of oceanic waters into the basin. The bathymetry of the southern Midland Basin and its proximal Sheffield Channel is poorly addressed in the literature. However, according to the reconstructions of Algeo and Heckel (2008), the Midland Basin may have been partially silled with respect to the connecting Sheffield Channel, due to the easterly extension of the Central Basin Platform and the Ozona Arch (Figure 2.3). This geographical configuration may have produced conditions amenable to deep water upwelling in the southern Midland Basin, assuming that the basin remained connected to the Panthalassic Ocean during times of sea-level lowstand. Numerical models by Castelão and Barth (2005) suggest that wind strength and bathymetric variations of the seafloor can lead to deep water upwelling associated with non-uniform sea floor topography. Because this project focuses solely on the Upton County core, it is difficult to pinpoint which of these mechanisms played the largest role in influencing basin-wide productivity. It is likely that a combination of factors helped to influence nutrient loading and export to the surface waters in the Midland Basin.

Erosion of the thermocline driven by wind shear across the basin as a possible mechanisms influencing primary productivity and organic facies development warrants an examination of the wind fields affecting the Midland Basin during Wolfcamp D time. During the Late Pennsylvanian, the super continent Pangea was coalescing and moving

into the northern hemisphere, which made climatic conditions highly variable (Rowley et al., 1985). The occurrence of a large land mass over the equator and the Midland Basin's proximity to the Panthalassic Ocean produces environmental conditions necessary for a seasonal monsoon in the low latitude tropics. Monsoonal conditions were set up by the differential heating of the midcontinent and the adjacent Panthalassic Ocean, which creates thermal and density contrasts driving seasonal winds carrying significant precipitation over the greater Permian Basin during Late Pennsylvanian time (Ruddiman, 2000). Parrish and Peterson (1988) provide some basic insights on wind patterns that influenced the Midland Basin during the climatic transition of the Late Pennsylvanian. Those authors indicate two possible controlling mechanisms for the winds, both of which would result in cross-basin air flow with the potential to generate internal mixing that enhances nutrient delivery and productivity in the Midland system. One option is for northwesterly winds, due to the proximity of the Panthalassic Ocean and monsoonal climatic conditions. A second option is northeasterly winds due to the presence of a tropical high pressure cell. Although the results of Parris and Peterson (1988) are somewhat equivocal, an important observation is that either northwesterly or northeasterly winds could blow obliquely across the long axis of the basin and create shear along the surface waters that drove upwelling, most likely on a seasonal basis. Such a mechanism potentially explains the presence of phosphate nodules, elevated wt. % TOC, and high biogenic silica in BMR1, which is interpreted as an important petroleum source rock in WC-D.

The composition of facies type BMR2 varies slightly in comparison to BMR1, though in hand sample these lithofacies are virtually indistinguishable. Facies type

BMR2 is distinguished from BMR1 by its major and trace element chemistry, as well as its vertical distribution in the core (Supplemental Figure 2). The most important chemical characteristic that defines BMR2 is its aluminum content. Observations of thin sections validate the XRF measurements, as clay content is higher in this facies (Figure 5.1). Like BMR1, the fabric of BMR2 is mostly massive and sedimentary structures are rare. Average wt. % TOC values are less than the BMR1 facies (average ~2.1 wt. % for BMR2 versus average ~3.1 wt. % for BMR1; Supplemental Table 1), but it is not unusual for BMR2 facies to exhibit organic richness at or exceeding what is typically favored for petroleum source rocks (Selley, 1985). Unlike BMR1, phosphate nodules are absent from BMR2, although pyrite is still relatively common as framboids, nodules, burrow fill, and lenses dispersed in the matrix. Scattered calcareous fossil hash, most likely derived from the shelf or slope, is also present in BMR2. Horizontal to sub-horizontal burrows have also been readily identified in BMR2.

Unlike BMR1, which is interpreted to be exclusively associated with a single position on the sea-level curve, BMR2 is slightly more diverse in its stratigraphic distribution. Deposition of BMR2 is interpreted to be associated with early rising stage and late falling stage of global eustatic sea-level. Increased %Al suggests that more detrital clays are being transported into the basin during times of relative sea-level rise. This could be attributed to re-mobilization of terrigenous material stored on the shelf during the rising stages of sea-level, or an alternative source of terrestrial sediment given that this position on the sea-level curve is coincident with melting continental glaciers and increased climatic variability (Mazzullo and Reid, 1989). Other lines of evidence, such as diminished organic matter, disrupted fabrics due to burrows, and pyrite content,

point to increased bottom water oxygenation, which is consistent with environmental conditions far different than the persistently anoxic and euxinic water bottom associated with the development of BMR1 (Bohacs, 1998; Boyer and Droser, 2009). Lowered TOC wt. % in the BMR2 facies suggests that organic matter preservation on the basin floor may have been hindered by bacterial decomposition, a process that can only occur in the presence of free oxygen (Sageman et al., 2003). Further, the decrease in pyrite in BMR2 suggests the redox front associated with this facies may have been at or below the sediment-water interface, increasing the amount of available oxygen in this benthic environment and sediment pore space (Bohacs 1998; Sageman et al., 2003). This position of the redox front and available free oxygen is favorable to the establishment of benthic organisms living in this oxic to sub-oxic environment and may be the cause for increased burrowing in the BMR2 facies.

The GMR facies type is often found in stratal contact with beds of BMR2 in the Upton County core (Supplemental Figure 2). Common microfabric and textural characteristics in this lithofacies includes wavy non-parallel discontinuous laminations of calcareous material. On occasion, scoured basal contacts can be identified in few locations within the core. Perhaps the most distinguishing characteristic of GMR is elevated calcium weight percentages relative to BMR1 and BMR2. We interpret this chemical signature to be the result of a higher fossiliferous debris (carbonate silt) and lime mud content. These features are readily observable in thin sections and in hand sample (Figure 4.1 and 4.2). The average aluminum values of the GMR facies type is ~5.8 wt. % (Supplemental Table 1). The %Al content falls in between BMR1 (average = 4.9 wt. %) and BMR2 (average = 7.0 wt. %).

The depositional process responsible for GMR is interpreted to be a combination of suspension settling and low concentration turbidity currents. Evidence for deposition from low density turbidity currents is provided by the erosive basal contacts of some GMR beds. This erosive contact is due to the turbulent flow regime associated with turbidity currents. In contrast to BMR1, which is interpreted to reflect lower depositional energy and a highly restricted Midland Basin at lowstand, lithological and chemical characteristics of GMR suggest deposition in a higher energy environment, most likely associated with early highstand or rising stage of global eustatic sea-level (Figure 5.2). The presence of lime mud in GMR suggest that the up-dip reef was either becoming active or beginning to shut down during the deposition of this facies type. This suggests that the up dip reefs were depositing mud into the basin during sea-level transitions or storm driven events (Loucks and Sarg, 1983). Carbonate deposition within the adjacent Delaware Basin has been presented far more extensively in the literature than the Midland Basin. This depositional system provides some potentially useful analogs for climatic, oceanographic, and tectonic gradients influencing facies development (Fisher and Sarnthein, 1988; Loucks and Sarg, 1993). The associated increase in fossiliferous material observed within GMR is interpreted to be an indication of a higher energy depositional regime and increased productivity of the up-dip reef. Beds of GMR are commonly associated with calcareous debrites and thicker turbidites in the Upton County drill core, which is consistent with the facies having a genetic linkage to gravity flows (Supplemental Figure 2).

Mixed (Mx) facies for the Upton County drill core shares chemical characteristics of black mudrocks and carbonates. For example, the average %Al for mixed facies is

~4.3 wt. %, which is less than average values for both BMR1 and BMR2. By contrast, average %Ca values for the mixed facies (~9.0 wt. %) are slightly higher than mean GMR values, but substantially lower than allochthonous carbonates (~ 27.0 wt. %). These chemical traits arise due to the fact that this facies is characterized by distorted, intercalated beds of multiple rock types. Frequently, this expresses in hand sample and thin section as wavy, tilted, or folded thin beds of BMR1 juxtaposed with diffuse and discontinuous laminations of carbonate debris (Figure 4.1h, Figure 4.2h and Figure 5.3).

Mixed facies types are interpreted to be either soft sediment deformation (e.g., slumping) or low density turbidites that have been transported downslope and deposited in the basin during transitional periods of sea-level (Shanmugam, 1997). Beds of the Mx lithofacies were found in close proximity to debris flow deposits near the top of the core (~183 ft; Figure 5.3). However, particularly low density carbonate turbidites lacking classic Bouma sequence structures are mostly found near the base of WC-D, before thicker and coarser carbonate turbidites and debrites mark the stratigraphic record with great frequency. This dilute low density turbidite expression of the Mx facies type is indicative of a lower stratal position in the core compared to soft sediment deformation higher in the core. Soft sediment deformation is marked by distorted lenses of black mudrocks intercalated with Ws and Ps (Figure 4.1, Figure 4.2, and Figure 5.3). This type of deposition may be the result of slumping, internal shear deformation created as debris flows or high density turbidity currents move down slope, or as soft sediment creep moving down slope (Owen, 1996; Rossetti, 1999; Potter et al., 2005; Chapin et al., 2014). An alternative interpretation for this irregular bedding architecture is differential compaction from overlying sediments, with water escaping from underlying muds,

creating a vertical shear component to the bed. However, this mechanism is less effective at explaining all of the attributes of the Mx facies (Owen, 1996; Rossetti, 1999; Chapin et al., 2014).

Carbonate lithofacies, including Ws, Ps, and Gs, constitute ~18% of the Upton County drill core. Grainstones consisted of fine calcareous silt and abraded fossiliferous debris, whereas Ws and Ps were much coarser with identifiable fossiliferous material separated by lime mud matrix. Facies types Ws and Ps contain fossils including bivalves, brachiopods, crinoids, foraminifera (fusulinids), gastropods, ostracods, and trilobites, only varying in the amount of mud matrix present. Facies Gs may also contain fossils from these fauna, but fragmentation and abrasion of the calcareous skeletons produced only very fine grains which were impossible to identify. Wackestone and Ps facies are present in comparatively thick beds (~1 - 7 ft), whereas beds of Gs are much thinner (< 1 ft). Grainstones exhibit normal grading on occasion, and internal laminations are common to abundant. We interpret that Gs facies were generated by turbidity currents of varying intensity due to the diversity of grain densities apparent in thin sections. Unlike Gs facies, the characteristics of Ws and Ps lithofacies are consistent with deposition by debris flows (Loucks and Sarg, 1993). The presence of mud matrix and dispersed skeletal grains common in WC-D Ws and Ps facies is similar to many gravity flow deposits (e.g., debrites) described from the deep water rock record from around the world. Shanmugam and Benedict (1978) provided a useful classification system to differentiate turbidites and debrites, which has been expanded upon by numerous authors, including Posamentier and Walker (2006) and Loucks and Sarg (1983) for carbonates. The Ws and Ps facies share a number of characteristics with submarine debris flow

deposits, including: (1) planar basal contacts absent of erosion; (2) a lack of long axis orientation of floating grains; and (3) projected clasts at the upper and lower contact of the surrounding sediment (Shanmugam and Benedict, 1978). Perhaps the most striking contrast between Ws, Ps, and Gs in our record is evidence of erosion. Grainstone beds, which are typically thinner and contain finer fossiliferous grains, commonly scour into underlying facies, whereas Ws and Ps beds exhibit much weaker evidence of erosion, interpreted to be the result of differences between turbulent and laminar flow (Figure 5.4).

Sea-level highstand conditions are interpreted to have produced Ws and Ps facies in the Upton County drill core. Following the interpretative framework of Sarg (1988), a transitional late highstand period is plausible for these deposits, just prior to the initial regression. If this interpretation is accurate, then carbonate gravity flows reflect shedding from the productive shelf reef complexes into the basin margin during the Late Pennsylvanian (Loucks and Sarg, 1983). Partially analogous to Late Quaternary carbonate deposition of the Bahama Banks, these low latitude platform margins rimming the Midland Basin have active carbonate factories during sea-level highstands, thus increasing the total productive area of the reef complex and derived sediment (Loucks and Sarg, 1983; Schlager et al., 1994), assuming that the reef is not deeply drowned, which would preclude reef growth due to a lack of sunlight. The increase in reef production leads to a larger volume of material susceptible to submarine erosion from wave activity and currents, thus increasing the amount of sediment available for transport by gravity flows and mass wasting (McIlreath, 1977). This down slope transport forms debris aprons that disrupt background sedimentation on the lower slope, toe of slope, and

basin floor (McIlreath, 1977; Loucks and Sarg, 1983). Potential analog environments in the rock record include the Boundary Limestone of the Southern Canadian Rocky Mountains, the Mount Hawk Basin in Alberta Canada, and the Delaware Basin of west Texas and eastern New Mexico (Cook et al., 1972; McIlreath, 1977, Loucks and Sarg, 1983).

By contrast, we interpret that the deposition of Gs turbidites at the Upton County site reflects the influence of rising and falling sea-level (Figure 5.4). Calcareous grainstones are most abundant in the Upper WC-D and overlying WC-C2 intervals. Following this mechanism, wave base lowers as sea-level regresses, and imparts energy to the outer shelf that allowed gravity flows to develop. The impact of the lowered wave base could result in erosive action that promotes slope instabilities and mass wasting (Shanmugam and Moiola, 1984), allowing for mobilization and transport of shelf derived carbonates onto the slope and deeper basin floor. There is evidence for neither subaerial exposure nor meteoric diagenesis in the Gs facies. Thin section analysis revealed that dissolution, cement formation, and dolomitization are absent.

Magnesium-rich limestone facies types are interpreted to be dolomite cement grounds, or omission surfaces, formed in association with extremely low sedimentation rates on the basin floor (Hillgärtner, 1998; McLaughlin, 2008). They are considered to represent the rising stage of global sea-level, due to rapid melting of continental ice sheets of Gondwana. This rapid transgression decreases the amount of sediment flushed into the deepest parts of the Midland Basin, creating an omission surface (Potter et al., 2005). These intervals are commonly associated with bioturbation, glauconite, and pyrite in the Upton County core (Figure 5.5). Similar facies characteristics have been identified

by McLaughlin et al. (2008) in condensed beds of the middle Proterozoic of eastern North America and by Hillgärtner (1998) in France and Switzerland associated with carbonate platforms.

The final lithofacies type identified for this study is the Diagenetic Mineralized Bed (DMB) facies type. Although the occurrence of this facies type in the Upton County drill core is scarce, its presence has value for paleo-environmental characterization of the basin. These beds vary in thickness but are usually <0.5 ft. Laminations composed of pyrite, in addition to beds of peloidal pyrite, glauconite, and phosphate nodules comprise the DMB facies in the Upton County drill core (Figure 4.5 and 4.6).

Peloidal pyrite, as described by Scheiber (1989) in the Chattanooga Shale, is the defining characteristic of this facies type. Microscopic observations of this facies via Dino-Lite ® images and hand lens have identified the pyrite morphology as peloidal (Figure 4.6). Scheiber (1989) notes that this morphology is representative of pyritized fecal pellets. Fecal pellets have not been observed in abundance for the WC-D, yet the morphology of these grains are consistent with a peloidal origin. Additionally, the presence of phosphatic particles are associated with this type of deposit described by Schieber (1989) and are observed here in the WC-D comparative beds. The most striking occurrence of this facies type is situated at ~284 ft, between beds of BMR1 (below) and BMR2 (above). This is interesting, as BMR1 represents a lowstand deposit, whereas BMR2 represents the onset of the rising stage of sea-level in the Midland Basin. The mechanism for the deposition of this facies type according to Schieber (1989) is winnowing and erosion of underlying muddy sediments, which may have occurred as transgression commenced. Also observed in these beds are a considerable amount of

glauconite. The presence of glauconite is harder to interpret, but they may be associated with penecontemporaneous remobilization of glaucony by storms during relative transgression (Amorosi, 1995; Amorosi, 1997; Schieber, 1989). Due to the color and grain morphology observed in these sediments it is believed that these sediments are allochthonous or parautochthonous detrital sediments (Amorosi, 1995; Amorosi, 1997).

Stratigraphic Evolution at the Upton County Site

The Upton County drill core is a stacked succession of alternating lithofacies dominated by mudrocks and allochthonous carbonates. Mudrocks throughout the core can be difficult to distinguish in hand sample or via digital image analysis alone. Integration of geochemical and petrophysical logs help to clarify important transitions in the facies. Allochthonous carbonate facies on the other hand differ quite dramatically, and are easier to discriminate in hand sample. The inclusion of fossils, as well as visible physical sedimentological features such as graded bedding and scour marks are much more obvious in carbonates than the massive, sparsely-laminated mudrocks. Wolfcampian rocks of the Permian Basin are known to be heterogeneous, and lower Wolfcamp deposits are commonly singled out for high frequency facies variability that exceeds overlying Wolfcamp and Sprayberry deposits (Hamlin and Baumgardner, 2012). However, a major finding of our analysis is that the WC-D at the Upton County core site is internally heterogeneous with respect to vertical facies stacking patterns.

Supplemental Figure 2 presents the integrated stratigraphy of the WC-D for the Upton County drill core. Using these data, we interpret three discrete depositional sub-units, herein named the Lower, Middle, and Upper WC-D. These three sub-units differ in stratal stacking patterns, distribution of lithofacies, and organic and inorganic

chemostratigraphy. These characteristics have been used to guide the interpretation of important environmental boundary conditions on the Midland Basin during WC-D time, with a special emphasis placed on understanding sea-level changes. Sea-level change, sediment supply dynamics, and tectonic influences on accommodation are important controls on deposition in mixed siliciclastic-carbonate depositional systems (Sarg, 2012; Bohacs, 1998; Schlager, 1994). An early hypothesis for this project centered on eustatic sea-level as a major driver of facies variability; our interpretations suggest that base level fluctuations influence patterns of mineralogy, organic enrichment, and carbonate gravity flow activity. This analysis was partially facilitated by convolving XRF-derived major and trace element chemistry data into principal components analysis, using the software PAST (Hammer and Harper, 2006). Using PCA and lithofacies, we have identified and characterized WC-D cycles based on physical and chemical characteristics for each interval (Supplemental Figure 3).

The Lower WC-D sub-unit is 68 ft thick and is comprised dominantly of BMR1, which accounts for ~ 45% of this interval. The Lower WC-D is from 325 - 257 ft in the core. Other mudrock facies are common in Lower WC-D, with GMR and BMR2 comprising ~20% and 15% of the sub-unit, respectively (Table 4.1). Grey mudrocks are conspicuous at both the top and bottom of the sub-unit, and as such may reflect transitional periods of increased clay and carbonate detritus entering the deep basin. As illustrated in Figure 5.6, black mudrocks in Lower WC-D are located in the lower and upper interval of this cycle and comprise a ~30 ft section of rock. Grey mudrocks are typically found between carbonate lithofacies in the middle of this sub-unit and measure 1-3 ft thick. These lithofacies sit both above and below M-Ls beds that are characteristic

of this interval. Dolostone lithofacies account for ~11% of the Lower WC-D interval, whereas carbonates (~9%) make up the balance. An interesting and noteworthy aspect of the Lower WC-D is a transition in black mudrocks. This mudrock facies transition occurs straddling a prominent, 2 in thick DMB bed (Figure 4.6). Below the DMB, a ~13 ft thick bed of BMR1 transitions vertically into a thinly interbedded package of BMR1 and BMR2, which underlies an M-Ls cement ground ~12 in thick. These lithofacies are overlain by the pyrite and glauconite DMB marker bed, above which grades into a carbonate debrite (Ws) with abundant glauconite and small phosphate nodules (Figure 5.7). One plausible explanation for this marked facies transition relates to an amplitude change on the global sea-level curve. As shown in Figure 2.2, the amplitude of sea-level change shifts near the top of the Lower Absaroka 1.3 and the base of the Lower Absaroka 1.4 Super Sequence sets (Sloss, 1963). As the dynamic range of sea-level increased, conditions favoring the development of BMR1 versus BMR2 may have responded sensitively. The weight of evidence suggests that BMR1 may be associated with sea-level lowstands, whereas lower trace metal and organic matter content in BMR2 appears to reflect recharge of bottom waters that may have accompanied greater mixing during initial transgression. Glauconite and phosphates are particularly prominent in this interval, which may be signaling the inception of a protracted transgression into Lower Absaroka 1.4, after which time the amplitude of sea-level changes became more extreme.

The Lower WC-D interval is interpreted to be one partial cycle of sea-level that extends into the Middle WC-D. This suggest a lower frequency of sea-level change for the Lower WC-D interval when compared the Middle and Upper WC-D intervals, which are interpreted to contain at least four and three complete cycles, respectively. The type

cycle for Middle WC-D shown in Figure 5.8 reflects a full eustatic period – facies patterns from lowstand trough to adjoining lowstand trough on the sea-level curve. Examination of the PCA (Supplemental Figure 3) aids in the identification of these sea-level cycles. Three principal components explain ~76% of the variance in the WC-D. The first principal component (explaining ~48% of the variance) loads positively on Si, Al, K, Ti and negatively on Ca, and we interpret these data to be a proxy for mineralogy. The second principal component (explaining ~17% of the variance) loads positively on Mo, Cr, Fe, and S, and weakly on Ti, K and Al, which we interpret as a redox proxy, with high values signaling restricted bottom waters that were anoxic and euxinic. The third principal component (explaining ~11% of the variance) loads on P and Mg, which tracks the presence of nodules and dolomitic cement grounds. The PCA data and the lithostratigraphic log make clear that the Lower WC-D interval has a different depositional expression than that of the overlying Middle and Upper WC-D sub-units (Supplemental Figure 2). The patterns shown in the PCA data define BMR1 deposition as prominent positive excursions of PC1 and PC2, which are strongly asymmetric near the base of Middle WC-D and become more symmetric and spike-like moving up section (Supplemental Figure 3). These data suggest that if sea-level controls the extent of bottom water restriction, then these changes occurred abruptly in Middle WC-D. By contrast, such changes appear to have occurred more progressively and with lower amplitude in Lower WC-D. Prominent PCA cycles are a hallmark of Middle WC-D. The muted nature of cycles in the Lower WC-D interval is interpreted to be a consequence of the transition from Lower Absaroka 1.3 into the Lower Absaroka 1.4 Super Sequence (Sloss, 1963). This transition is defined by a change in the amplitude of

eustatic changes, which suggests that a bathymetric threshold impacting bottom water redox may have been crossed in Middle WC-D. We hypothesize that an oceanographic gateway between the Midland Basin and Panthalassa may have been maintained at lowstand during Lower WC-D time, whereas complete restriction of the Midland Basin perhaps occurred as sea-level dropped below the elevation of the sill during the Middle and Upper WC-D. Future research integrating datasets with better spatial coverage may help to resolve this outstanding question.

Total organic carbon data for Lower WC-D show that the most organic rich rocks in this sub-unit are associated with the BMR1 facies type (Figure 4.8 and 4.9). This evidence is further corroborated by the spectral gamma ray curve, which tracks natural radioactivity via U, Th, and K content of the rocks. Additionally, principle component analysis demonstrates that intervals enriched in Fe, S, Mo, and Cr are also associated with the BMR1 facies type (Supplemental Figure 3). Together, these data suggest that BMR1 was deposited during periods of bottom water anoxia and possibly euxinia, conditions associated with a restricted water mass (Sageman et al., 2003; Algeo and Maynard, 2003; Algeo and Heckel, 2008).

The Middle WC-D is an 80 ft (~257-177 ft) interval containing at least four complete sea-level cycles (Figure 5.8). Middle WC-D is interpreted as particularly characteristic of the overall depositional style of lower Wolfcamp deposits in the southern Midland Basin. The Middle WC-D sub-unit exhibits well-defined, cyclic deposition of black mudrocks and allochthonous carbonate material derived from up-dip platform reefs, which is consistent with icehouse conditions. Sea-level lowstands are interpreted to be defined by thin to moderately thick beds of BMR1, whereas highstand conditions

are most commonly captured by thin Gs. However, within this interval vertical variability in mudrock composition is observed, with BMR1 becoming less common moving towards the upper sub-unit boundary. This pattern is interpreted to be an overall decline in the length of deep bottom water restriction or diminished sedimentation rates, consistent with the idea of a starved basin during the Late Pennsylvanian (Galley, 1958; Frenzel et al., 1988). The spectral gamma ray logs for this interval become increasingly spiky towards the top of the interval. This contrasts with the broad, asymmetric gamma peaks associated with cycles two and three of the lower Middle WC-D (Supplemental Figure 3). Carbonate lithologies found in the Middle WC-D interval consist of a few Gs beds and few fine-grained Ws beds toward the top of the interval.

The second principle component for Middle WC-D indicates a step-wise decrease in the magnitude and duration of bottom water restriction moving up section. A strong positive correlation exists between certain trace metals (Mo, Cr) and TOC in Middle WC-D (Figure 4.8 and 4.9) mudrocks, which is frequently indicative of euxinia (Sageman et al., 2003; Algeo and Maynard, 2004). Scatter plots of these geochemical parameters show that Middle WC-D is characterized by the strongest trace metal-TOC covariance patterns observed in the Upton county core (Figure 4.8 and Figure 4.9).

The Upper WC-D interval is the most heterogeneous sub-unit in the stratigraphy with respect to the vertical stacking of lithofacies. This interval is ~73 ft thick (177 - 104 ft) and it is interpreted to contain three complete sea-level cycles. All facies types are present in this interval, but particularly prominent are the first appearance of thick, coarse debris flow deposits (Ws and Ps). Another important characteristic of Upper WC-D are very thin beds of BMR1 (typically < 1 ft), whereas BMR2 beds are thicker (~2 ft

average) and much more numerous. The type cycle for this interval is ~30 ft thick and includes a thick, coarse debrite (Figure 5.9). These Ws debrites contain pebble sized-grains that include fossils, intraclasts, and mud clasts that are often rimmed with calcium carbonate. A characteristic feature of these debrites are the lack of erosive bases due to laminar flow, as well as occasional projected clasts found at both the lower and upper contact of the bed (Shanmugam and Benedict, 1978). Usually found in close proximity to debris flows are thinly bedded (< 1 ft) calcareous turbidites. These turbidites rarely display the full suite of Bouma-type beds, but most exhibit scoured bases, basal normal grading, parallel laminations, and convolute laminations (Shanmugam, 1997). The provenance of these carbonate gravity flow deposits cannot be precisely determined due to the nature of our dataset. Nevertheless, possible triggering mechanisms that may have initiated gravity flows include: (1) earthquakes; (2) differential uplift of the Central Basin Platform; (3) over-steepening of the platform margin due to tectonic deformation; or (4) over production of the carbonate factory itself (Cook et al., 1972). Tectonic activity near the Upton County core could be related to movement on local faults, which maps developed by Pioneer Natural Resources indicate may have been active during deposition of WC-D (Waite, personnel communication, 2015). These processes, when combined with storms and sea-level variability, could potentially drive mass wasting events that impact the depositional record of the deep basin. Organic geochemistry of the Upper WC-D interval indicates that mudrocks are generally less rich in TOC than the underlying Middle WC-D mudrocks, which may be a function of dilution by clay (reflected in the higher %Al) and carbonate, as well as preservation dynamics associated with less sustained deep water anoxia. This is not to suggest that Upper WC-D does not

contain BMR1; in fact, the single highest TOC wt. % measurement in the dataset resides in this sub-unit. Total organic carbon values for this interval vary from 0.1-7.5 wt. %. Trace metal correlations to TOC for the Upper WC-D interval are correlated to both Cr and Mo (Figure 4.8 and 4.9). These correlations for the Upper WC-D sub-interval are stronger than the Lower WC-D interval but weaker than the Middle WC-D sub-interval

Sea-level Dynamics

The working interpretation favored for eustatic sea-level controls on facies change in the Midland Basin during the Late Pennsylvanian time is that BMR1 facies is associated with the lowstand limb of the sea-level curve, whereas carbonate gravity flow deposits are associated with sea-level highstands (Figure 5.10, 5.11, and 5.12). An alternate interpretation, centered on highstand organic enrichment is possible however, though it is not as strongly supported by the data available for the project. The alternative interpretation places the BMR1 facies in a highstand position on the sea-level curve, with shedding of the carbonate platform associated with regressions. The shape of the PC2 curve lends some support to this interpretation, especially near the base of the Middle WC-D interval, where cycles are strongly asymmetric and marked by an abrupt initiation. Assumptions based on modern analogs suggest that abrupt changes in sea-level would most likely be associated with deglaciation and sea-level transgression (Ruddiman, 2001). By contrast, regressions would progress more slowly, as glacial ice built on the continents. If the variables that describe the PC2 curve (Mo, Cr, Fe, S) are dominantly controlled by sea-level, then it follows that abrupt positive changes may reflect sea-level highstands; it is these intervals that are marked by deposition of BMR1. However, some issues arise with this alternate model. For example, many tropical

Quaternary rimmed carbonate platforms experience shedding during times of relative sea-level highstand (Crevello and Schlager, 1980; Schlager et al., 1994). If we assume that the Midland Basin's carbonate platforms were exposed during times of sea-level lowstand, evidence for meteoric diagenesis would have been observed in thin section analysis of the carbonate material in the core. Additionally, with the carbonate platform exposed, production would be shut down and the active reef would migrate to the slope and occupy only a thin narrow marginal area around the basin (Loucks and Sarg, 1983). Moreover, platform sediments become quickly lithified when exposed to fresh water and as winnowing occurs during the fall of sea-level (Crevello and Schlager, 1980; Schlager et al., 1994). This migration of the carbonate platform to the slope of the basin would reduce the occupied area of the platform and thereby the volume of transported material into the basin would be expected to decrease. According to Schlager (1994), only one example of carbonate lowstand shedding from turbidite aprons around Pacific atolls has been reported. This work, conducted by Thiede and Thiede et al. (1981), was later revisited by Dolan (1989), who concluded that the deposits "…developed in response to establishment of a shallow-water source area rather than as a direct result of eustatic sea-level changes. Other occurrences appear to record highstand shedding of shelf sediment…" Evidence for lowstand shedding of carbonate systems in the geologic record are therefore scarce, and as such we favor the highstand model for allodapic carbonate facies development.

Petroleum Geology

The results of this study have implications for unconventional oil reservoir characterization. The WC-D interval consists of alternating lithologies with two different

types of black, organic-rich mudrock. We interpret the BMR1 facies, the most organically enriched mudrock in the Upton county core, as potential unconventional oil reservoirs. The inorganic chemical make-up of BMR1 appears to be suitable for drilling and hydraulic fracturing, due to the low relative %Al and high %Si content of the rock (Figure 5.1). Three possible horizons have been identified as possible targets for unconventional horizontal wells. These targets exhibit favorable reservoir characteristics defined by this study including: (1) organic richness above ~2 wt. % TOC; (2) thick vertical sections of BMR1; and (3) inorganic geochemical properties that suggest mineralogy that will respond in a brittle fashion in response to applied stresses. Consequently, these targets are the first three complete cycles identified if the Upton County drill core (Supplemental Figure 3). The first target resides in the Lower WC-D sub-interval, while cycles two and three are the first two cycles contained within the Middle WC-D sub-interval.

The first target identified in the Lower WC-D sub-interval lies at a core depth range of 297-284 ft (~13 ft). This horizon within the Lower WC-D sub-interval is 98.6% BMR1, with %TOC values ranging from 1.6 to 4.4 (Supplemental Figure 2). Sone and Zoback (2013) demonstrated using laboratory experiments that the ductile properties and brittle strength of shale reservoirs are dependent on material composition and sample anisotropy. Therefore, we use Si:Al as an indicator of mineralogy and geomechanical behavior (Figure 5.1). As %Si is our mineralogical proxy for quartz (brittle) and %Al our mineralogical proxy for clay (ductile), high values of Si:Al suggest that inducing fractures could be best achieved in mudrocks with these properties. The Si:Al values for this horizon are between 4.1 and 13.5, making it the most brittle target identified.

The second horizon identified as a possible unconventional target is the first cycle within the Middle WC-D sub-interval. This horizon lies in the depth range of 249 - 236 ft (Supplemental Figure 1, 2, and 3). This target is ~13 ft thick and consists of 88.5% BMR1. Total organic carbon for this horizon is ~2.9 - 6.3 wt. % TOC. The amount of rock separating this interval from the one below is ~35 ft. Si:Al values for this potential reservoir range from 4.3 to 7.1. This target interval is the type cycle chosen for the Middle WC-D sub-interval and has been classified as the number one target for drilling based on %TOC data.

A third target horizon identified in this study is the second cycle within the Middle WC-D sub-interval (Supplemental Figure 3). This horizon is ~6 ft thick, and lies at a depth of 224 - 218 ft. This target consists of 100% BMR1 with %TOC data ranging from 3.5 to 5.6 wt. %. Si:Al values for this horizon vary from 5.3 to 8.0. This final target sits ~12 ft above the target below. Depending on the efficacy of hydraulic fracture propagation, these shallower intervals may be accessible by one lateral well fracturing both targets, thus increasing the productivity of the well and reducing total drilling costs. The dominant and most abundant lithofacies separating these two target locations are GMR and BMR2.

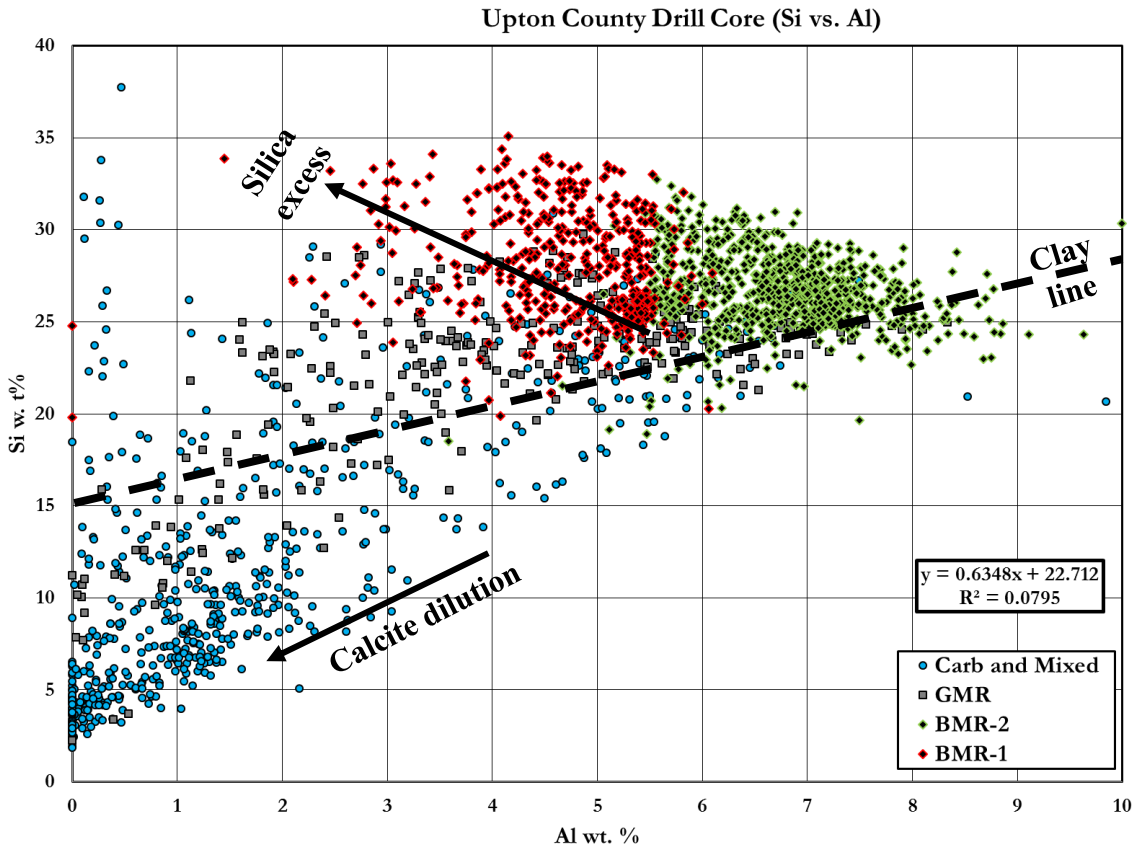

Figure 5.1. %Si vs. %Al Upton County Drill Core.
XRF-derived cross plot of silicon versus aluminum values for the entire Upton County Drill Core. The data have been further divided by facies. A clear division can be seen in the data cloud near~5.5-6 %Al. Almost all black mudrock lithofacies consist of %Si values greater than 20 and less than 35. The silica excess line is thought to be due to biogenic silica and trace detrital silica input. Additionally, the GMR facies occupies Si/Al space between the carbonate and mudrock facies, an intrinsic characteristic of this facies type. The strong linearity between %Al and %Si at lower concentration are believed to indicate dilution by calcite and the influence of the Bruker calibration (Rowe et al., 2008).

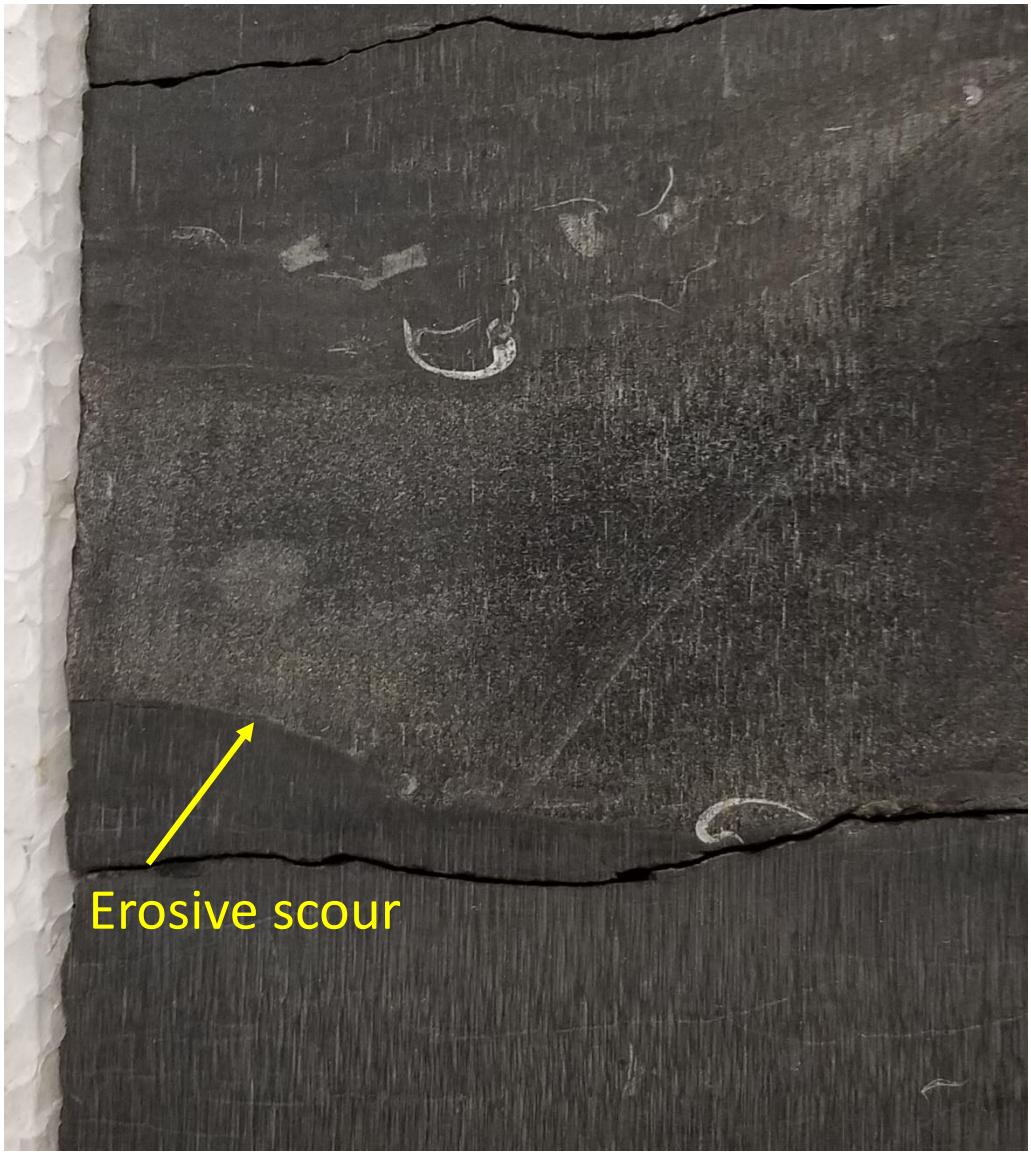

Figure 5.2. Grey Mudrock with Erosive Scour.
Grey mudrock of the Upton County Drill Core exhibiting an erosive scour mark due to turbulent flow. The GMR lithofacies is interpreted to be a product of sea-level transition and is genetically related to Ws, Ps, and Gs.

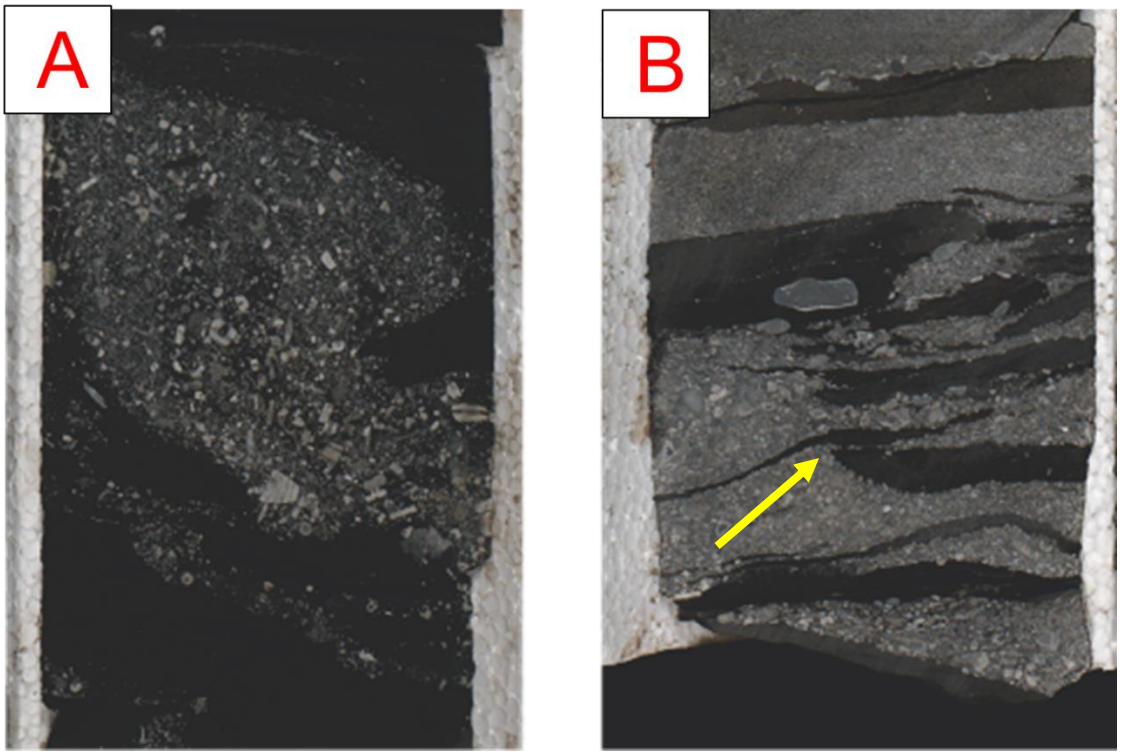

Figure 5.3. Mixed (Mx) Lithofacies Examples.
Two examples of the Mx lithofacies type found in the Upton County Drill Core. A) Photo shows misshapen crinoid fossil debris with round bedding contacts. Calcareous sediment in this photo has either been deposited non-horizontally or was distorted after deposition. B) Core box photo of distorted beds due to shear stress generated by overriding high density turbidity currents or a pebble debris flow. The yellow arrow points to a shear induced asymmetric rippled wackestone/packstone facies.

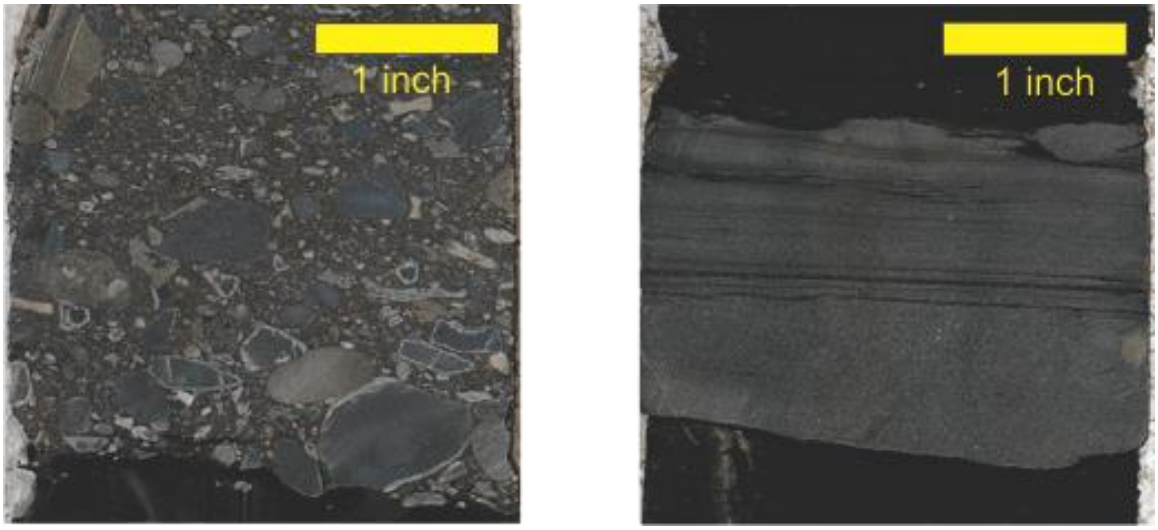

Figure 5.4. Debrite vs. Turbidite
Core photograph of debrite (left) and turbidite (right). The debrite displays pebble to cobble sized clasts supported by a mud matrix. Basal contacts do not exhibit strong erosive boundaries, however clasts are projected into the underlying mud. The long axis orientation of grains in this type of deposit is a key characteristic of flow dynamics. The turbidite does display an erosive basal contact with grain sizes too small to identify macroscopically. Internal laminations and grading consistent with the Bouma sequence interpretation.

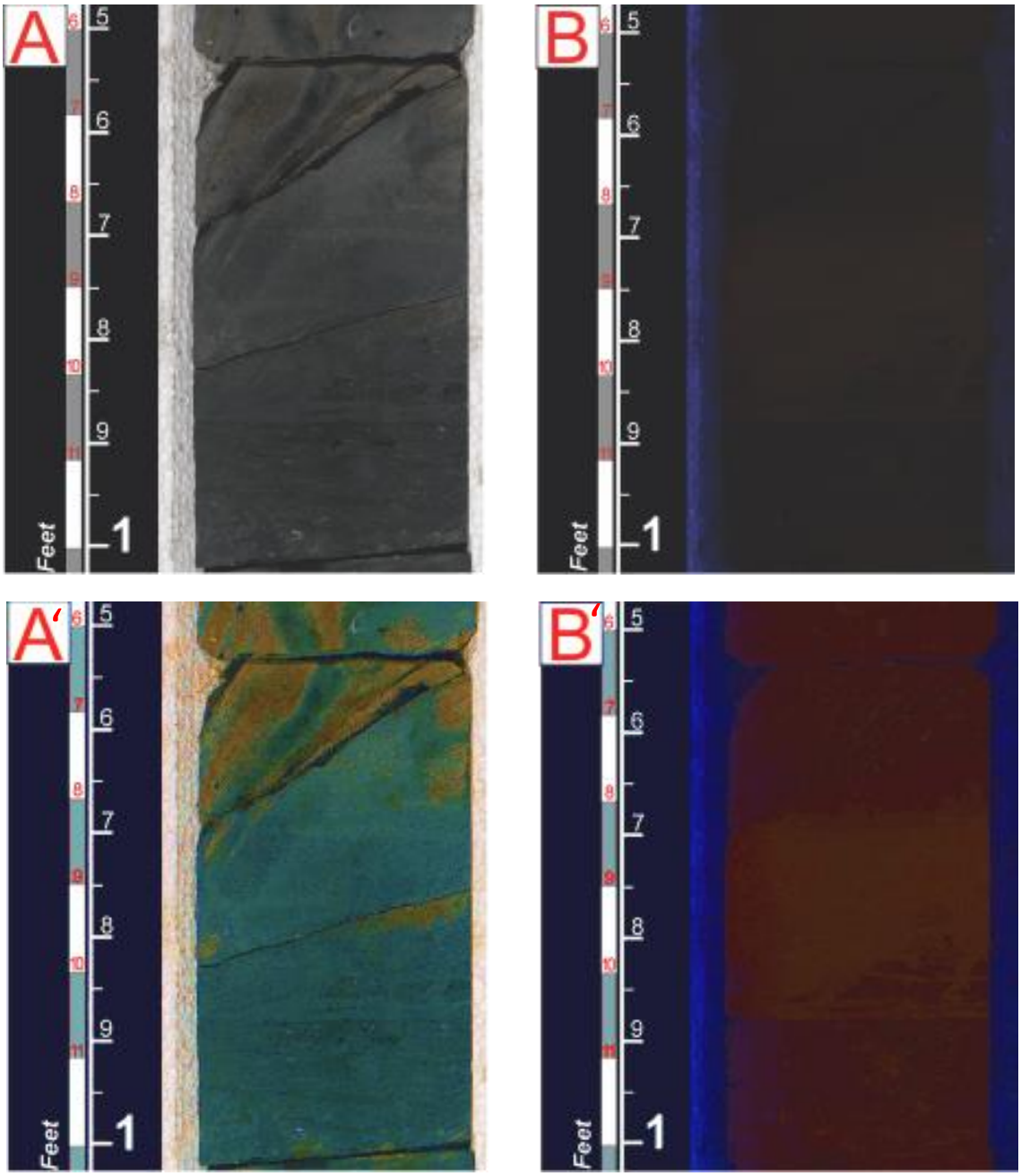

Figure 5.5. Dolomite Lithofacies (M-Ls).
A) Dolomite lithofacies in plane light exhibiting horizontal burrows and a gradational contact from the underlying mud. The contrast has been set to 100% in order to identify key characteristics of this lithofacies type (A' and B'). B) Same image under UV light, note faint orange glow. Saturation set to 100% to display the burrows more readily.

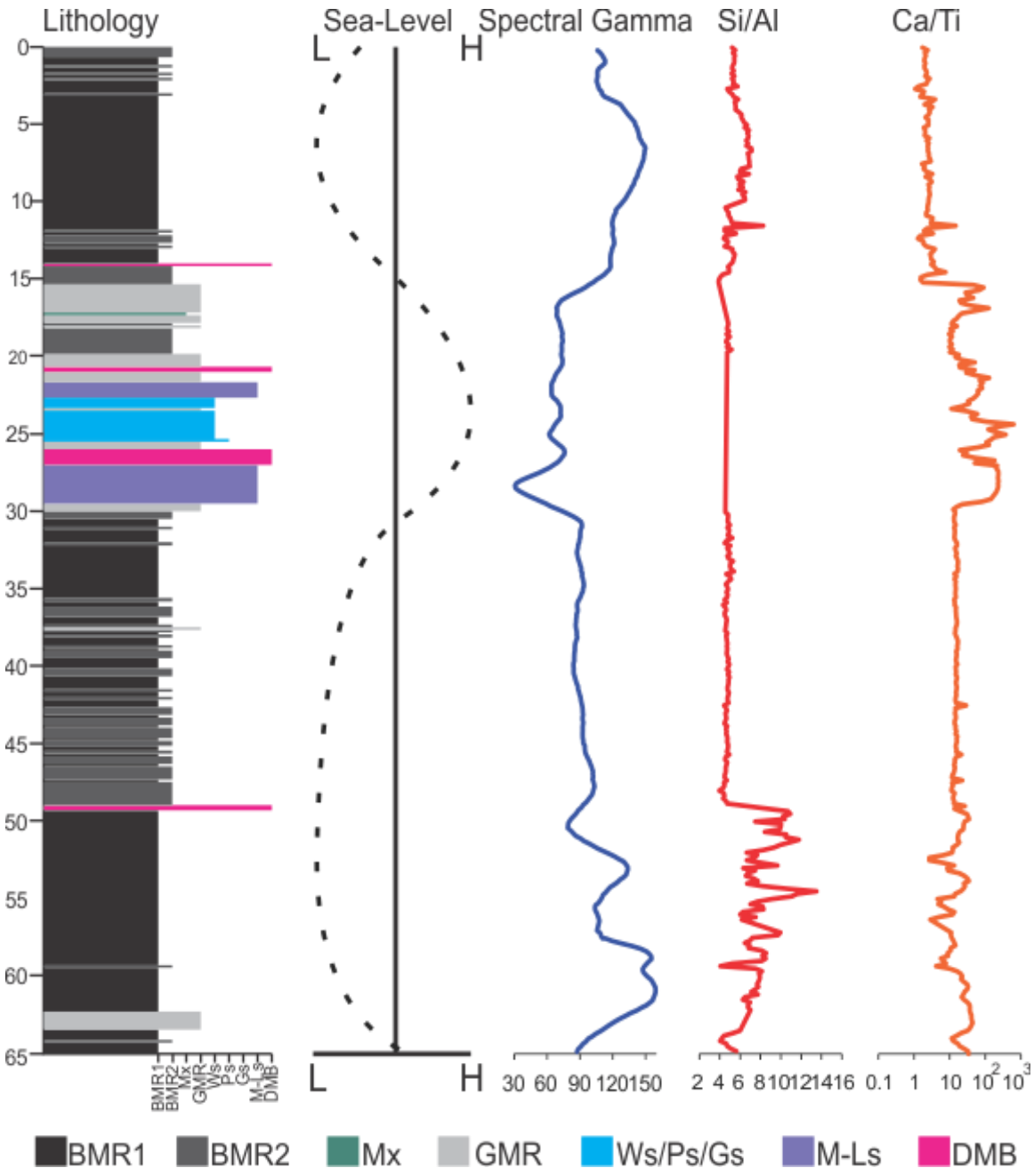

Figure 5.6. Lower Wolfcamp D Type Cycle for Upton County Drill Core.
The type cycle for the Lower WC-D sub-unit consists of thick beds of BMR1 overlain by interbeded BMR1 and BMR2. These rocks represent the lowstand and rising stage intervals of sea-level, respectively. Stratigraphically above these units sits a relatively thick M-Ls lithofacies that grades into a Ws bed. These intervals represent a rapid rise in sea-level and high stand to late highstand, respectively. The cycle concludes by returning to the BMR1 lithofacies type.

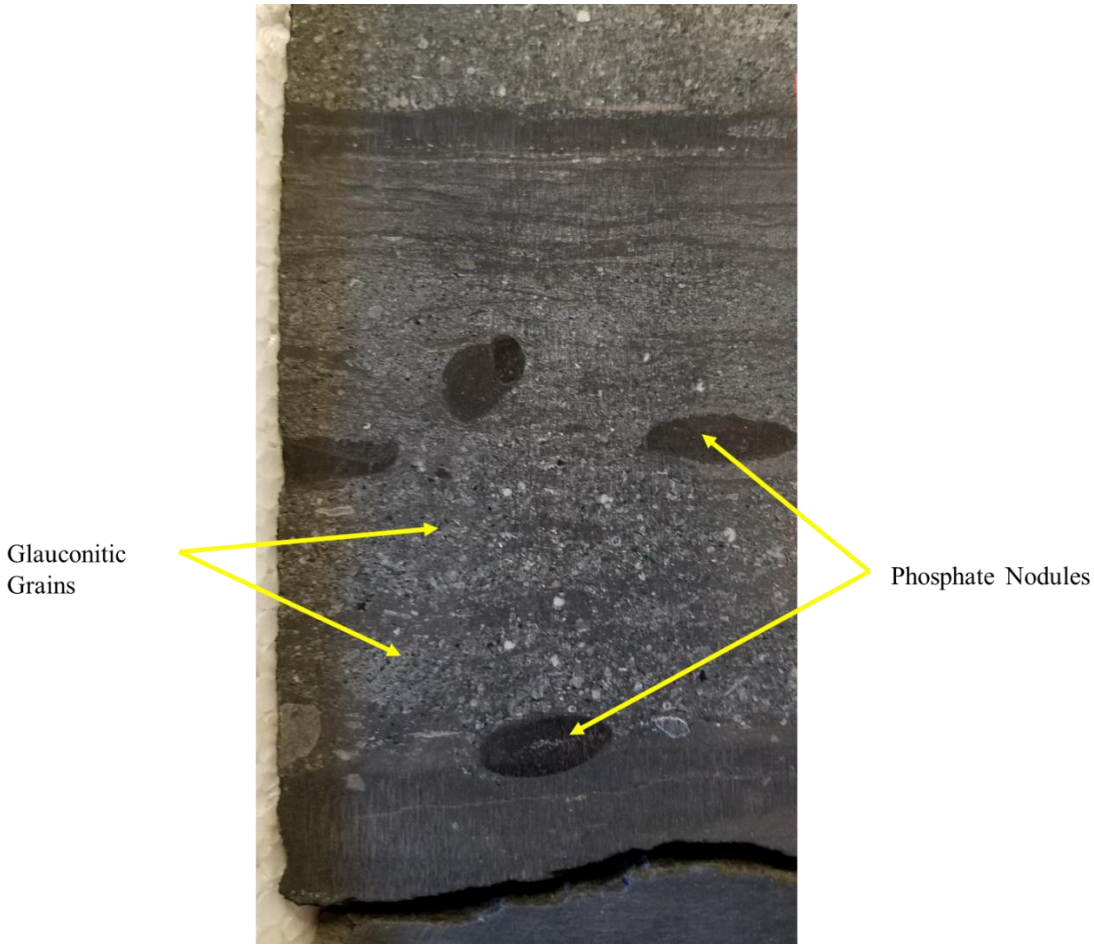

Figure 5.7. Gravity flow depositwith Diagenetic Grains.
This pebble to sand-sized turbidite consists of fossiliferous debris, glauconitic grains, and phosphate nodules. Interestingly, the phosphate nodules do not displace sedimentary features within the flow, suggesting they were transported along with the other constituents of the flow. Glauconitic grains are dark green and exhibit sub-angular to sub-rounded grain boundaries.

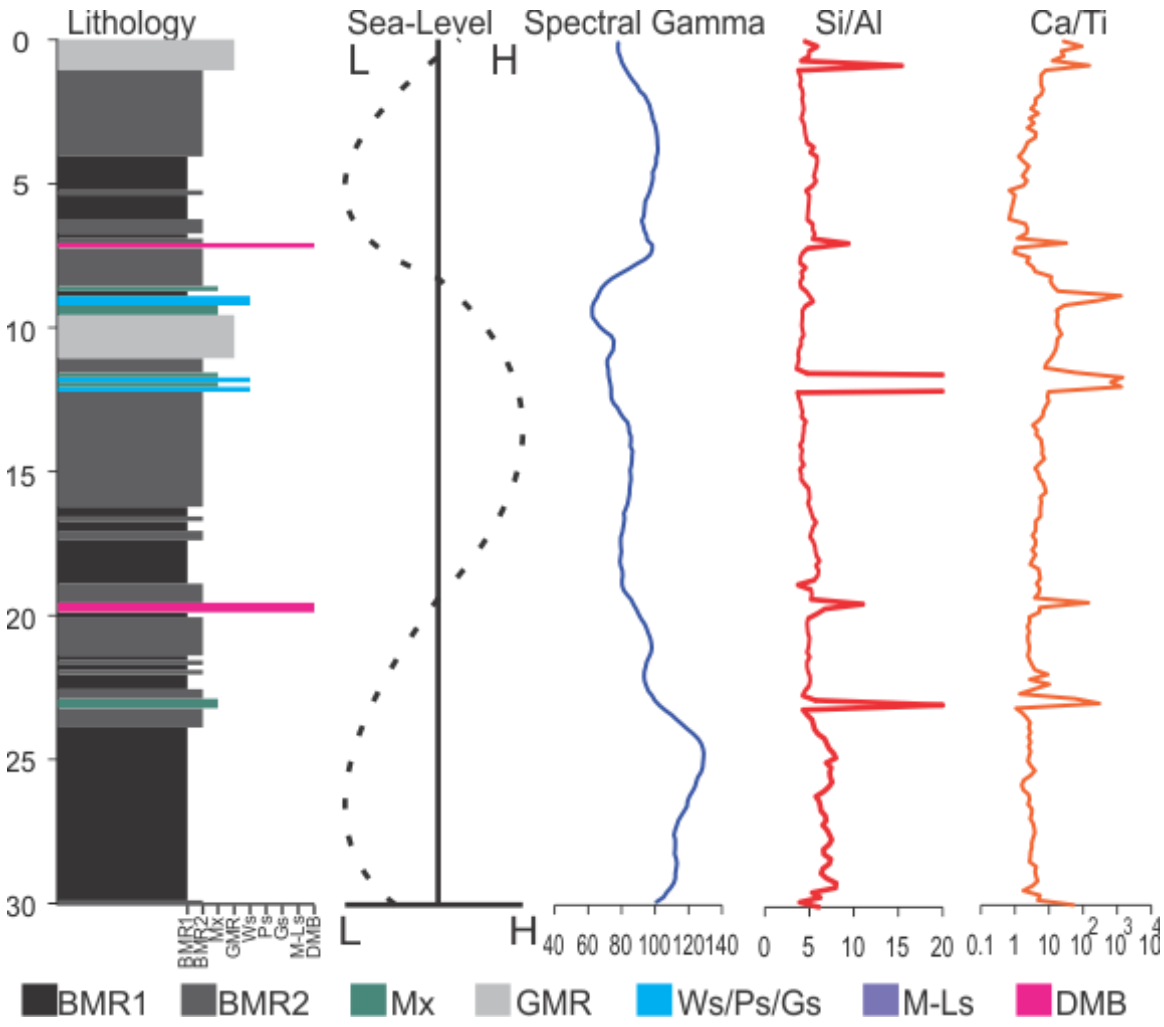

Figure 5.8. Middle Wolfcamp D Type Cycle.
The MWC-D sea-level cycle begins with a lowstand marked by a representative ~8 ft thick section of BMR1. As in the LWC-D type cycle, BMR1 is overlain by BMR2. Additionally, scarce traces of the Mx lithofacies as well as DMB lithofacies are present. The DMB appears to be a signal of sea-level transition and trangression. Highstand deposition of calcareous material is thin within this interval. However, the GMR package situated between two beds of Ws is a signal of high stand in this package. The cycle is complete in the thinner BMR1 lithofacies at ~5 ft depth.

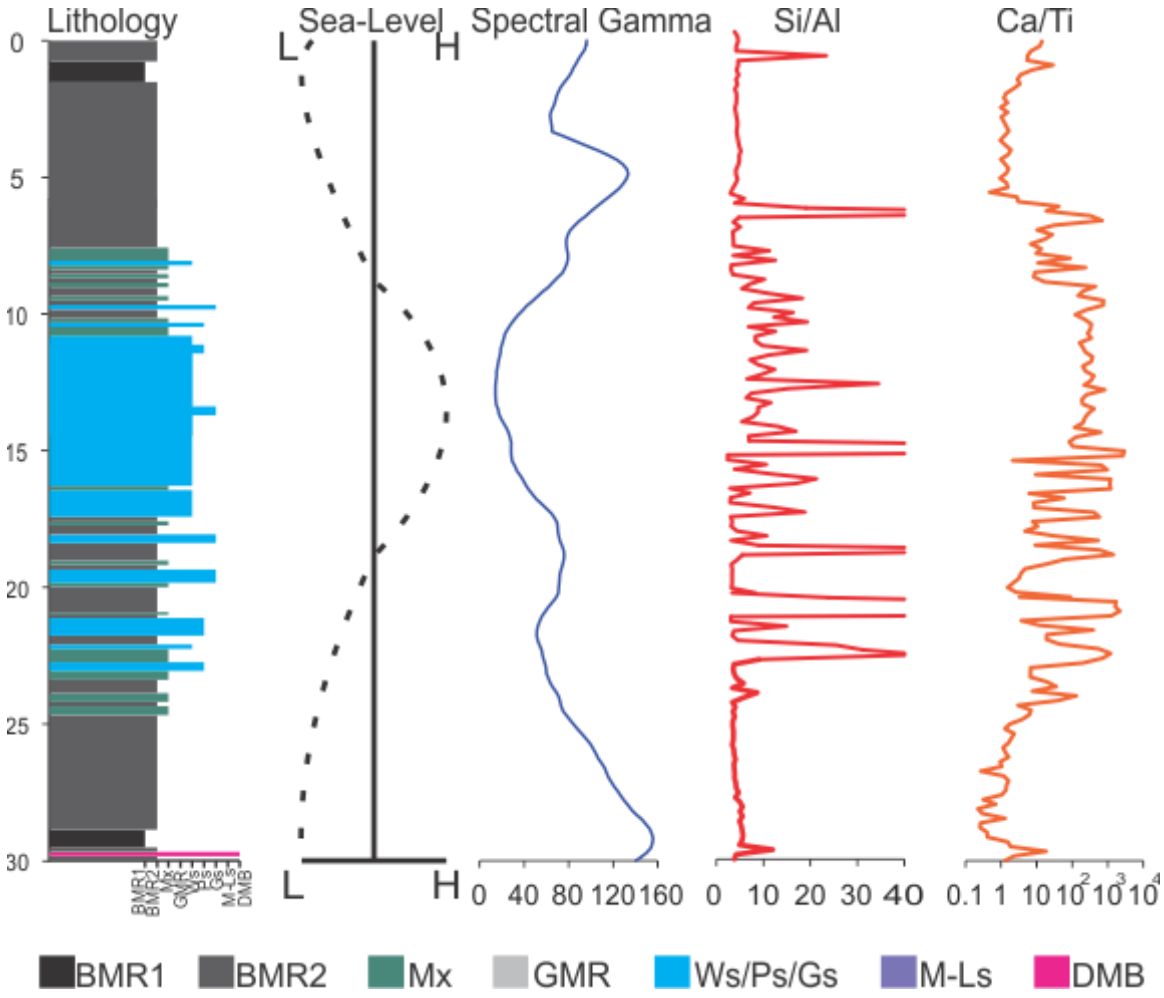

Figure 5.9. Upper Wolfcamp D Type Cycle.
The last sub-unit of the WC-D has a dramatically different expression of sea-level cycles, but it still begins and ends with thin beds of BMR1. The rising stage of sea-level is marked by thin Ps to Gs turbidites. Highstand deposition contains thick packages of Ws and thinly bedded Ps. Remarkably, this interval is almost absent of the BMR1 lithofacies and has been replaced by BMR2.

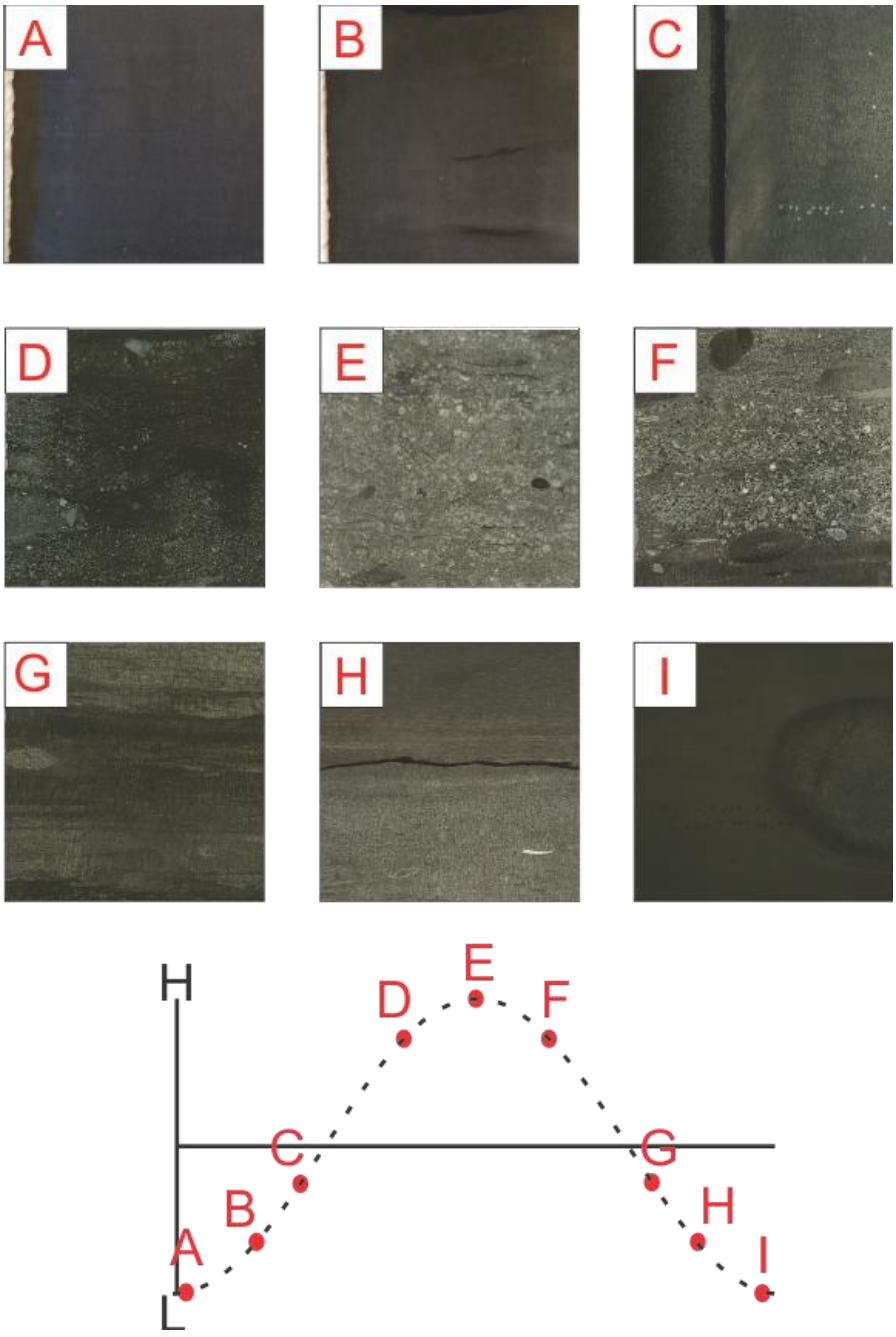

Figure 5.10. Conceptual Model of Sea-level for the LWC-D.
A model of sea-level change and the response of the sediment types in the core. Panel A, B, and I are BMR1; a golf ball sized phosphate nodule can be seen in panel I. Panel C is an M-Ls, exhibiting a blocky vertical fracture. Panel D is a DMB lithofacies preceding the derites of panel E and F (See Figure 5.8). Panel G is the Mx lithofacies of low density turbidity flows lacking Bouma sequence style bedding. Panel H display the contact of GMR (below) and BMR1 (above).

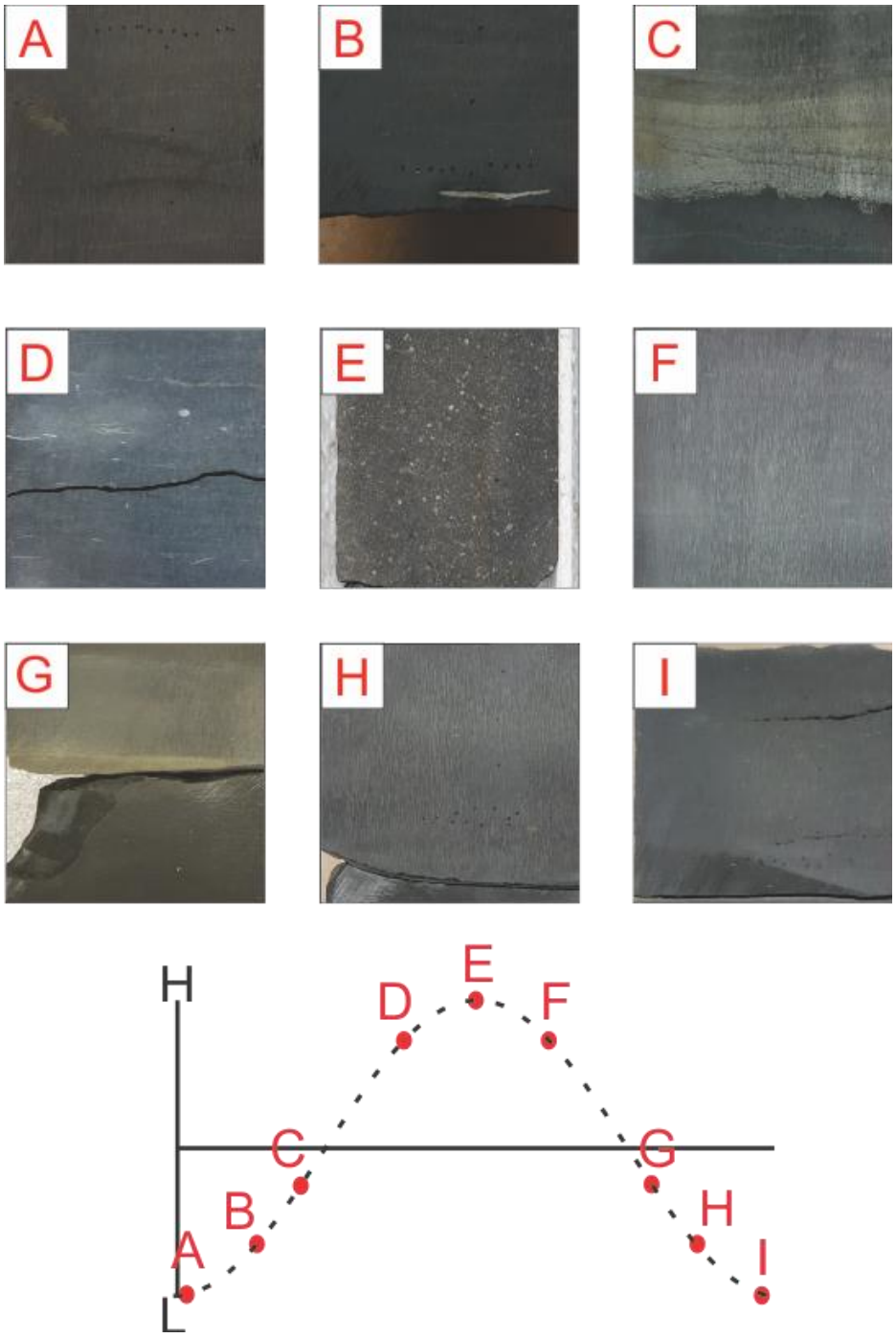

Figure 5.11. Conceptual Model of Sea-level for the MWC-D.
As in the LWC-D type cycle, panels A and I are the BMR1 lithofacies type. Panel B is the BMR2 lithofacies. Panels C and G are thinly bedded DMB lithofacies. These thin beds consist of calcareous pyritic laminations. Panel D is the GMR lithofacies with increased fossiliferous debris and extreme dilute turbidity flows. Panel E is a silty calcareous Ws lithofacies. Grains in this image are silt to sand sized and mud supported. Panel F and H are the BMR2 lithofacies (See Figure 5.9).

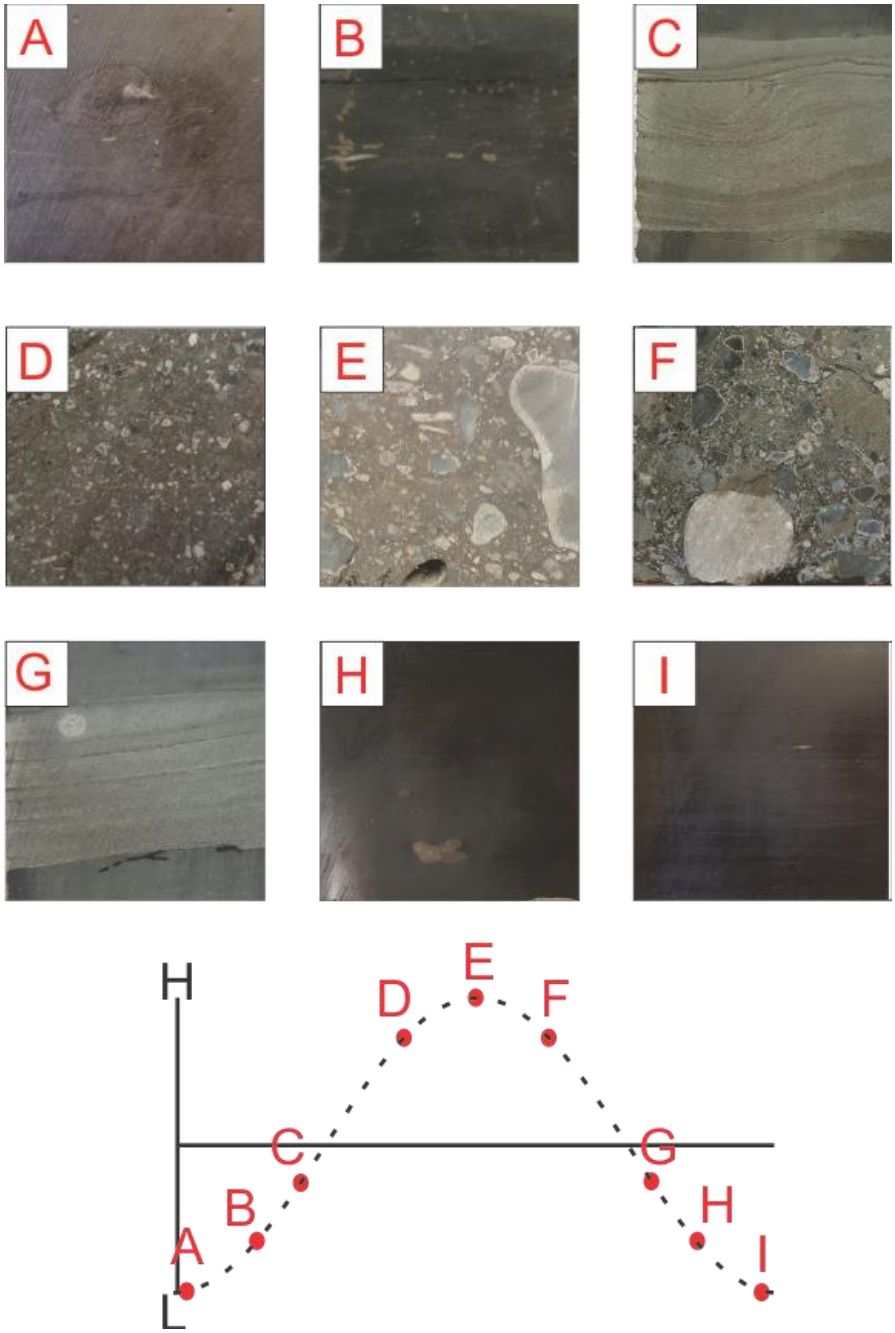

Figure 5.12. Conceptual Model of Sea-level for the UWC-D.
Panels A and I are BMR1 lithofacies. Panel A displays a 1 inch diameter phosphate nodule in the center of the image, whereas panel I shows shows a small pyrite nodule. Panel B and H are the BMR2 lithofacies and present pyritized burrows and nodules respectively. Panels D, E, and F displays the varying size of grains present in debris flows in the UWC-D. Panel C and G is a classic Gs turbidite with an erosive basal contact and internal wavy laminations.

CHAPTER 6: CONCLUSIONS

Integrated stratigraphic analyses conducted for this study provide some of the first insights on the depositional character of WC-D in the southern Midland Basin. The data demonstrate that WC-D is characterized by significant stratigraphic and geochemical variability in vertical section, which is interpreted to be controlled by environmental gradients dominantly associated with eustacy.

- Stratal stacking patterns, the distribution of lithofacies, and inorganic and organic geochemistry allowed the WC-D to be divided into lower, middle, and upper sub-units. The characteristic depositional style of the WC-D is highly cyclic and consists of periods of background hemi-pelagic sedimentation intermittently interrupted by calcareous gravity flows. However, the characteristics of the cycles vary depending on stratal level.
- Nine distinct lithofacies occur in the WC-D, and the most abundant types are Al-rich black mudrock (BMR2) and Si-rich black mudrock (BMR1). In the Upton County drill core, the frequency of carbonate lithofacies (gravity flow deposits) changes moving up section. A key threshold was crossed at ~170 ft, as above this level, carbonate turbidites and debrites become much more common. The character of gravity driven carbonate deposition also changes above ~170 ft. Bed thickness and grain-size of allochthonous carbonate sediments increase in the Upper WC-D and overlying WC-C2 when compared to the Lower and Middle WC-D.
- Mudrock lithofacies also vary vertically in the Upton County core. Whereas BMR1 is the dominant mudrock lithofacies below ~170 ft (lower half of WC-D),

BMR2 lithofacies is dominant above ~170 ft (upper half of WC-D and WC-C2). This transition suggests that sediment delivery to the core location changed at the ~170 ft stratal level, and favored the delivery of detrital clays to the core site in upper WC-D and WC-C2.

- The weight of evidence generated by the integrated stratigraphic analysis suggests that the organic-rich BMR1 facies accumulated when sea-level was at relative lowstand. During regression events, shelf carbonate factories either shut down or migrated to the slope margin, thereby significantly decreasing the amount of allochthonous carbonate delivered to the basin floor by gravity flows and mass wasting. In the deepest parts of the basin, sea-level lowstands favored pervasive anoxia and likely euxinia, which allowed for organic matter preservation in lithofacies deposited under these conditions. These rocks, represented by BMR1, likely obtained their high %Si due to surface water productivity, perhaps associated with upwelling. Conversely, periods of sea-level highstand are marked by increased carbonate shedding from the surrounding platforms. The Ws lithofacies are interpreted to be ancient debris flows that mark highstands of eustatic sea-level, whereas BMR2, GMR, and Gs lithofacies constitute periods of sea-level transition. The onset of sea-level transitions are often marked by DMB lithofacies. During periods of rapid sea-level transgression and slow sedimentation in deepwater, basin floor sediments experienced diagenesis and cementation. This resulted in the formation of the M-Ls facies, which are common in the lower and middle WC-D sub-units.

- Nine cycles of glacio-eustatic sea-level have been identified within the WC-D using principal component analysis integrated with lithofacies. Of these nine cycles, three have been identified as possible targets for unconventional petroleum reservoirs. These targets are located in the Lower WC-D and near the base of the Middle WC-D sub-units. Targets consist of thick packages (~8-13 ft) of organically enriched (average TOC is ~3.1 wt. %) BMR1 lithofacies marked by high relative values of Si:Al. Total organic carbon content is positively correlated with the concentrations of Mo and Cr in BMR1, which indicates restricted bottom waters characterized by infrequent mixing. Importantly, the abundance of the BMR1 lithofacies type decreases up section, and as a result, so does average TOC. The increased occurrence of BMR2 above ~170 ft (upper half of the WC-D and WC-C2) suggests the rocks contain more clays, less organic matter, and lack geomechanical properties favorable for hydraulic fracturing.

References

Algeo, T. J., & Heckel, P. H. (2008). The Late Pennsylvanian midcontinent sea of North America: a review. Palaeogeography, Palaeoclimatology, Palaeoecology, 268(3), 205-221.

Algeo, T. J., & Maynard, J. B. (2004). Trace-element behavior and redox facies in core shales of Upper Pennsylvanian Kansas-type cyclothems. Chemical geology, 206(3), 289-318.

Algeo, T. J., & Rowe, H. (2012). Paleoceanographic applications of trace-metal concentration data. Chemical Geology, 324, 6-18.

Amorosi, A. (1995). Glaucony and sequence stratigraphy: a conceptual framework of distribution in siliciclastic sequences. Journal of Sedimentary Research, 65(4).

Amorosi, A., (1997). Detecting Compositional, Spatial, and Temporal Attributes of Glaucony: A Tool for Provenance Research. Sedimentary Geology, (109)1, 135-153.

Aplin, A. C., & Macquaker, J. H. (2011). Mudstone diversity: Origin and implications for source, seal, and reservoir properties in petroleum systems. AAPG bulletin, 95(12), 2031-2059.

Boardman, D. R., & Heckel, P. H. (1989). Glacial-eustatic sea-level curve for early Late Pennsylvanian sequence in north-central Texas and biostratigraphic correlation with curve for midcontinent North America. Geology, 17(9), 802-805.

Bohacs, K. M., Lazar, O. R., & Demko, T. M. (2014). Parasequence types in shelfal mudstone strata—Quantitative observations of lithofacies and stacking patterns, and conceptual link to modern depositional regimes. Geology, 42(2), 131-134.

Bohacs, K. M. (1998). Contrasting expressions of depositional sequences in mudrocks from marine to non-marine environs.

Bohacs, K. M. (1990). Sequence stratigraphy of the Monterey Formation, Santa Barbara County: Integration of physical, chemical, and biofacies data from outcrop and subsurface.

Boyer, D. L., & Droser, M. L. (2009). Palaeoecological patterns within the dysaerobic biofacies: Examples from Devonian black shales of New York state. Palaeogeography, Palaeoclimatology, Palaeoecology, 276(1), 206-216.

Bridge, J., Barnes, V. E., & Cloud, P. E. (1947). Stratigraphy of the upper Cambrian, Llano uplift, Texas. Geological Society of America Bulletin, 58(1), 109-124.

Brown, L. F., (1969). Virgil and Lower Wolfcamp Repetitive Environments and the Depositional Model, North-central Texas. Bureau of Economic Geology, University of Texas at Austin.

Budzik, P., & Perrin, J., (2014). Six formations are responsible for surge in Permian Basin crude oil production. Retrieved October 09, 2015, *from* http://www.eia.gov/todayinenergy/detail.cfm?id=17031#.

Campbell, C. V. (1967). Lamina, laminaset, bed and bedset. Sedimentology, 8(1), 7-26.

Castelao, R. M., & Barth, J. A. (2006). The relative importance of wind strength and along-shelf bathymetric variations on the separation of a coastal upwelling jet. Journal of physical oceanography, 36(3), 412-425.

Chapin, M. A., Brandon, N. W., Ugueto, G., & Govert, A. (2014). Sedimentology and reservoir characterization of the Upper Cretaceous Lance and Upper Mesaverde intervals from core data in Pinedale field, Wyoming.

Cook, H.E. et al., (1972). Allochthonous Carbonate Debris Flows at Devonian Bank ('reef') Margins Alberta, Canada. Bulletin of Canadian Petroleum Geology, 20(3), 439-497.

Crevello, P.D., & Schlager, W., (1980). Carbonate Debris Sheets and Turbidites, Exuma Sound, Bahamas. Journal of Sedimentary Petrology, 50(4).

Crowell, J. C. (1978). Gondwanan glaciation, cyclothems, continental positioning, and climate change. American Journal of Science, 278(10), 1345-1372.

Dolan, J. F. (1989). Eustatic and tectonic controls on deposition of hybrid siliciclastic/carbonate basinal cycles: discussion with examples. AAPG Bulletin, 73(10), 1233-1246.

Dunham, R. J. (1962). Classification of carbonate rocks according to depositional textures.

Dutton, S. P., Kim, E. M., Broadhead, R. F., Raatz, W. D., Breton, C. L., Ruppel, S. C., & Kerans, C. (2005). Play analysis and leading-edge oil-reservoir development methods in the Permian basin: Increased recovery through advanced technologies. AAPG bulletin, 89(5), 553-576.

U.S. Energy Information Administration - EIA - Independent Statistics and Analysis. (n.d.). Retrieved October 10, 2015, from http://www.eia.gov/petroleum/.

Ettensohn, F. R., Miller, M. L., Dillman, S. B., Elam, T. D., Geller, K. L., Swager, D. R., ... & Barron, L. S. (1988). Characterization and implications of the Devonian-Mississippian black shale sequence, eastern and central Kentucky, USA: Pycnoclines, transgression, regression, and tectonism.

Fisher, A.G. & Sarnthein, M., (1988). Airborne Silts and Dune-Derived Sands in the Permian of the Delaware Basin. Journal of Sedimentary Petrology, 58(4), 637-643.

Flügel, E. (2004). Microfacies of carbonate rocks: analysis, interpretation and application. Springer.

Frenzel, H. N., Bloomer, R. R., Cline, R. B., Cys, J. M., Galley, J. E., Gibson, W. R., ... & Thompson III, S. (1988). The Permian basin region. Sedimentary cover—North American craton: US: Boulder, Colorado, Geological Society of America, The Geology of North America, 2, 261-306.

Galley, J. E. (1958). Oil and geology in the Permian basin of Texas and New Mexico: North America.

Gaswirth, S.B., Marra, K.R., Cook, T.A., Charpentier, R.R., Gautier, D.L., Higley, D.K., Klett, T.R., Lewan, M.D., Lillis, P.G., Schenk, C.J. & Tennyson, M.E., (2013). Assessment of undiscovered oil resources in the bakken and three forks formations, Williston Basin Province, Montana, North Dakota, and South Dakota. US Geological Survey Fact Sheet, 3013(4).

Garcés, B. L. V., Gierlowski-Kordesch, E., & Bragonier, W. A. (1997). Pennsylvanian continental cyclothem development: no evidence of direct climatic control in the Upper Freeport Formation (Allegheny Group) of Pennsylvania (northern Appalachian Basin). Sedimentary Geology, 109(3)305-319.

Hamlin, H.S. & Baumgardner, R.W., (2012). Wolfberry (Wolfcampian-Leonardian) Deep-Water Depositional Systems in the Midland Basin: Stratigraphy, Lithofacies, Reservoirs, and Source Rocks. Bureau of Economic Geology, Jackson School of Geosciences, University of Texas at Austin, Austin, Texas.

Hammer, Ø. & Harper, D.A.T. (2006). Paleontological Data Analysis. Blackwell. Hammer, Ø., Harper, D.A.T., and P. D. Ryan, 2001. PAST: Paleontological Statistics Software Package for Education and Data Analysis. Palaeontologia Electronica, 4(1), 9.

Heavens, N.G., Mahowald, N.M., Soreghan, G.S., Soreghan, M.J. & Shields, C.A., (2015). A model-based evaluation of tropical climate in Pangaea during the late Palaeozoic icehouse. Palaeogeography, Palaeoclimatology, Palaeoecology, 425, 109-127.

Heckel, P. H. (1977). Origin of phosphatic black shale facies in Pennsylvanian cyclothems of mid-continent North America. AAPG Bulletin, 61(7), 1045-1068.

Heckel, P. H. (1986). Sea-level curve for Pennsylvanian eustatic marine transgressive-regressive depositional cycles along midcontinent outcrop belt, North America. Geology, 14(4), 330-334.

Hillgärtner, H., (1998). Discontinuity Surfaces on a Shallow-Marine Carbonate Platform (Berriasian, Valanginian, France and Switzerland). Journal of Sedimentary Research, 68(6), 1093-1108.

Hoak, T., Sundberg, K., & Ortoleva, P. (1998). Overview of the structural geology and tectonics of the Central Basin Platform, Delaware Basin, and Midland Basin, West Texas and New Mexico (No. DOE/PC/91008--23-Pt. 8). Science Applications International Corp., Germantown, MD (United States).

Huffman Jr, A. C. (2003). Middle Pennsylvanian tectonics of the conterminous United States.

Jacobs, T. (2013). Cracking the Cline: A New Shale Play Develops in the Permian Basin. Journal of Petroleum Technology, 65(11), 70-77.

Jarvie, D. M., Hill, R. J., Ruble, T. E., & Pollastro, R. M. (2007). Unconventional shale-gas systems: The Mississippian Barnett Shale of north-central Texas as one model for thermogenic shale-gas assessment. AAPG bulletin, 91(4), 475-499.

Kidder, D. L. (1985). Petrology and origin of phosphate nodules from the Midcontinent Pennsylvanian Epicontinental Sea. Journal of Sedimentary Research, 55(6).

Lorenz, J. C., Sterling, J. L., Schechter, D. S., Whigham, C. L., & Jensen, J. L. (2002). Natural fractures in the Spraberry Formation, Midland basin, Texas: The effects of mechanical stratigraphy on fracture variability and reservoir behavior. AAPG bulletin, 86(3), 505-524.

Loucks, R. G., & Sarg, J. F. (Eds.). (1983). Carbonate Sequence Stratigraphy: Recent Developments and Applications, AAPG Memoir 57 (No. 57). AAPG.

Loucks, R. G., Reed, R. M., Ruppel, S. C., & Hammes, U. (2012). Spectrum of pore types and networks in mudrocks and a descriptive classification for matrix-related mudrock pores. AAPG bulletin, 96(6), 1071-1098.

Marshall-Neill, G., & Ruffell, A. (2004). Authigenic phosphate nodules (Late Cretaceous, Northern Ireland) as condensed succession microarchives. Cretaceous Research, 25(4), 439-452.

Mazzullo, S.J., & Reid A.M., (1989). Lower Permian Platform and Basin Depositional Systems, Northern Midland Basin, Texas. SEPM Special Publication, 44, 305-320.

McIlreath, I. A. (1977). Accumulation of a Middle Cambrian Deep Water Limestone Debris Apron Adjacent to a Vertical Submarine Carbonate Escarpment Southern Rocky Mountains Canada.

McLaughlin, P. I., Brett, C. E., & Wilson, M. A. (2008). Hierarchy of sedimentary discontinuity surfaces and condensed beds from the middle Paleozoic of eastern North America: implications for cratonic sequence stratigraphy. Geological Association of Canada Special Paper, 48, 175-200.

Munsell, A. H., (1954). Munsell Soil Color Chart. Munsell Color Co., Baltimore, MD.

Owen, G. (1996). Experimental soft-sediment deformation: structures formed by the liquefaction of unconsolidated sands and some ancient examples. Sedimentology, 43(2), 279-293.

Parrish, J. T., & Peterson, F. (1988). Wind directions predicted from global circulation models and wind directions determined from eolian sandstones of the western United States—A comparison. Sedimentary Geology, 56(1), 261-282.

Posamentier H.W., & Walker R.G., (2006). Deep-Water Turbidites and Submarine Fans. *in* Posamentier H.W., and Walker R.G., Facies Models Revisited. SEPM Special Publication, 84, 397-520.

Potter, P. E., Maynard, J. B., & Depetris, P. J. (2005). Mud and mudstones: Introduction and overview. Springer Science & Business Media.

Pratt, L. M. (1984). Influence of paleoenvironmental factors on preservation of organic matter in Middle Cretaceous Greenhorn Formation, Pueblo, Colorado. AAPG Bulletin, 68(9), 1146-1159.

Ring, E., (1989). The preperation and certification of fourteen South African silicate rocks for use as a reference materials. MIntek Report M393.

Rossetti, D.F., (1999). Soft-Sediment Deformation Structures in Late Albian to Cenomanian Deposits, São Luís Basin, Northern Brazil: Evidence for Paleoseismicity. Sedimentology, 46, 1065-1081.

Rowe, H. D., Loucks, R. G., Ruppel, S. C., & Rimmer, S. M. (2008). Mississippian Barnett Formation, Fort Worth Basin, Texas: Bulk geochemical inferences and Mo–TOC constraints on the severity of hydrographic restriction. Chemical Geology, 257(1), 16-25.

Rowe, H., Hughes, N., & Robinson, K. (2012). The quantification and application of handheld energy-dispersive x-ray fluorescence (ED-XRF) in mudrock chemostratigraphy and geochemistry. Chemical Geology, 324, 122-131.

Rowley, D. B., Raymond, A., Parrish, J. T., Lottes, A. L., Scotese, C. R., & Ziegler, A. M. (1985). Carboniferous paleogeographic, phytogeographic, and paleoclimatic reconstructions. International Journal of Coal Geology, 5(1), 7-42.

Ruddiman, W. F. (2001). Earth's Climate: past and future. Macmillan.

Sageman, B. B., Murphy, A. E., Werne, J. P., Ver Straeten, C. A., Hollander, D. J., & Lyons, T. W. (2003). A tale of shales: the relative roles of production, decomposition, and dilution in the accumulation of organic-rich strata, Middle–Upper Devonian, Appalachian basin. Chemical Geology, 195(1), 229-273.

Sarg, J.F., (1988). Carbonate Sequence Stratigraphy. *in* Sea-Level Changes—An Integrated Approach. SEPM Special Publication. 42, 155-181.

Scott, C., & Lyons, T. W. (2012). Contrasting molybdenum cycling and isotopic properties in euxinic versus non-euxinic sediments and sedimentary rocks: refining the paleoproxies. Chemical Geology, 324, 19-27.

Schieber, J. (1996). Early diagenetic silica deposition in algal cysts and spores: a source of sand in black shales?. Journal of Sedimentary Research, 66(1).

Schieber, J. (1998). Sedimentary features indicating erosion, condensation, and hiatuses in the Chattanooga Shale of Central Tennessee: relevance for sedimentary and stratigraphic evolution (pp. 187-215).

Schieber, J., & Zimmerle, W. (1998). Petrography of shales: a survey of techniques. Shales and mudstones: petrography, petrophysics, geochemistry, and economic geology, 2, 3-12.

Schlager, W., Reijmer, J. J., & Droxler, A. (1994). Highstand shedding of carbonate platforms. Journal of Sedimentary Research, 64(3).

Selley, R.C., (1985). Elements of Petroleum Geology: Second Edition. 24-28 Oval Road, London, Academic Press.

Shanmugam, G. (1997). The Bouma sequence and the turbidite mind set. Earth-Science Reviews, 42(4), 201-229.

Shanmugam, G., & Benedict III, G. L. (1978). Fine-grained carbonate debris flow, Ordovician basin margin, southern Appalachians. Journal of Sedimentary Research, 48(4).

Shanmugam, G., & Moiola, R. J. (1984). Eustatic control of calciclastic turbidites. Marine Geology, 56(1-4), 273-278.

Shumaker, R. C. (1992). Paleozoic Structure of the Central Basin Uplift and Adjacent Delaware Basin, West Texas (1). AAPG Bulletin, 76(11), 1804-1824.

Sloss, L. L. (Ed.), (1988). Sedimentary Cover—North American Craton: US. Geological Society of America.

Smith, L.B. & Read, J.F., (2000). Rapid onset of Late Paleozoic glaciation of Gondwana: Evidence from Upper Mississippian strata of the Midcontinent, United States. Geology; 28(3), 279-282.

Sone, H., & Zoback, M. D. (2013). Mechanical properties of shale-gas reservoir rocks—Part 2: Ductile creep, brittle strength, and their relation to the elastic modulus. Geophysics, 78(5), D393-D402.

Staplin, F. L. (1969). Sedimentary organic matter, organic metamorphism, and oil and gas occurrence. Bulletin of Canadian Petroleum Geology, 17(1), 47-66.

Tabor, N.J., Poulsen, C.J., (2008). Paleoclimate across the Late Pennsylvanian-Early Permian Tropical Paleolatitudes: A review of Climate Indicators, their Distribution, and Relation to Paleophysiographic Climate Factors. Paleogeography, Paleoclimatology, Paleoecology, doi:10.1016/j.paleo.2008.03.052.

Taylor, K. G., & Macquaker, J. H. S. (2000). Early diagenetic pyrite morphology in a mudstone-dominated succession: the Lower Jurassic Cleveland Ironstone Formation, eastern England. Sedimentary Geology, 131(1), 77-86.

Thiede, J. (1981). Reworked neritic fossils in upper Mesozoic and Cenozoic central Pacific deep-sea sediments monitor sea-level changes. Science, 211(4489), 1422-1424.

Thiede, J., Boersma, A., Schmidt, R. R., & Vincent, E. (1981). Reworked fossils in Mesozoic and Cenozoic pelagic central Pacific Ocean sediments, Deep Sea Drilling Project sites 463, 464, 465, and 466, leg 62. Initial Reports of the Deep Sea Drilling Project, 62, 495-512.

Veevers, J. T., & Powell, C. M. (1987). Late Paleozoic glacial episodes in Gondwanaland reflected in transgressive-regressive depositional sequences in Euramerica. Geological Society of America Bulletin, 98(4), 475-487.

Waite, L., Woodruff, O., McGlue, M., Baldwin, P., (2014). Unraveling the Wolfcamp D shale of the Midland Basin: Regional setting, initial geologic observations, and ongoing studies. Pioneer Natural Resources Internal Document.

Waite, L. & Read, T., (2014). Unraveling the Wolfcamp D interval in the Midland Basin: Initial observations. New Plays and Shale Technology Team. Pioneer Natural Resources.

West, R. R., Archer, A. W., & Miller, K. B. (1997). The role of climate in stratigraphic patterns exhibited by late Palaeozoic rocks exposed in Kansas. Palaeogeography, Palaeoclimatology, Palaeoecology, 128(1), 1-16.

Yang, K. M., & Dorobek, S. L. (1995). The Permian basin of west Texas and New Mexico: tectonic history of a" composite" foreland basin and its effects on stratigraphic development. Stratigraphic evolution of foreland basins: SEPM Special Publication, 52, 149-174.

VITA

Patrick Webster Baldwin

Education

B.S. Geology (2013)

University of North Carolina at Charlotte

A.A Arts (2011)

Rowan-Cabarrus Community College

Experience

Graduate Research Assistant

Paleoenvironments and Stratigraphy Lab

Department of Earth and Environmental Sciences

University of Kentucky, 40506

Graduate Teaching Assistant

Department of Earth and Environmental Sciences

University of Kentucky, 40506

Developmental Mathematics Instructor

Department of Mathematics

Rowan-Cabarrus Community College, 28027

Undergraduate Teaching Assistant

Department of Geography & Earth Sciences

University of North Carolina at Charlotte, 28223

Undergraduate Teaching Assistant
Department of Mathematics and Statistics
University of North Carolina at Charlotte, 28223